Supplementary Information for:

"Structural Characterization of the $[CuOR]^{2+}$ Core"

V. Mahesh Krishnan‡, Dimitar Y. Shopov‡, Caitlin J. Bouchey, Wilson D. Bailey, Riffat Parveen, Bess Vlaisavljevich,* and William B. Tolman*

TABLE OF CONTENTS

General Comments

Unless otherwise indicated, all reagents were purchased from commercial sources. All experiments were carried out under inert atmosphere in a N_2-filled glovebox or under Ar using Schlenk techniques; all glassware was oven-dried at 160 °C or flame-dried prior to use. UV-vis spectra were obtained using an HP8453 (190-1100 nm) diode array spectrophotometer equipped with a Unisoku low temperature cell holder. Kinetic data were analyzed using ReactLab KINETICS.[1] Cyclic voltammetry (CV) experiments were performed on an EC Epsilon potentiostat from BASi using a three-electrode cell comprised of a freshly polished Pt or glassy carbon (GC) working electrode, Pt counter electrode, and Ag wire pseudoreference electrode submerged in THF or CH_2Cl_2 with 0.2M tetrabutylammonium hexaflurophosphate (NBu_4PF_6, TBAP) as the electrolyte and either acetylferrocene (AcFc) or decamethylferrocene (Fc*) as an internal standard. The electrolyte, TBAP, was recrystallized several times from ethanol and dried overnight under high-vacuum before use. All potentials were referenced against the ferrocenium/ferrocene (Fc/Fc^+) redox couple using independent measurements (THF) or known $E_{1/2}$ values (CH_2Cl_2).[2] Unless otherwise noted, all solvents were purified and degassed with argon via a solvent system using alumina columns and dispensing directly into the glovebox. 1,2-difluorobenzene (DFB) was purified over acidified $KMnO_4$, dried with CaH_2, degassed via 4 freeze-pump-thaw cycles, collected via vacuum distillation, and subsequently stored in a glovebox over 3A activated molecular sieves. Ferrocenium tetra(3,5-bis-trifluoromethylphenyl)borate ($FcBAr^F{}_4$) was prepared using reported procedure.[3] Acetylferrocenium tetrakis[3,5-bis(trifluoromethyl)phenyl]borate ($AcFcBAr^F{}_4$) and [NBu_4][L^HCuOH] were prepared as described.[4,5] Dimethyl 4-methoxypyridine-2,6-dicarboxylate was prepared following a reported procedure.[6] Lithium 2,6-diisopropylanilide

(LiNHdipp) was prepared by addition of *n*-BuLi to a solution of 2,6-diisopropylaniline in pentane; the resulting precipitate was collected via filtration, washed with pentane, and used without further purification. 2,4,6-tri-*tert*-butylphenol (^{ttb}PhOH) was triply recrystallized from a saturated pentane solution at -30 °C prior to use. Elemental Analysis (CHN) was performed by the CENTC Elemental Analysis Facility (University of Rochester). Nuclear magnetic resonance (NMR) spectroscopy experiments were performed with either Varian Unity Inova (500 MHz) or Varian 300 MHz spectrometers; all deuterated solvents (chloroform-*d* ($CDCl_3$), dichloromethane-d_2 (CD_2Cl_2, CH_2Cl_2-d_2), 1,2-dichlorobenzene-d_4 (DCB-d_4)) were purchased from Cambridge Isotope Laboratories or Sigma-Aldrich, degassed, and dried over activated 3A molecular sieves prior to use. EPR simulations were performed using the EasySpin EPR simulation package, v. 5.1.[7] Experimental details regarding X-ray crystallography and resonance Raman spectroscopy are provided in their respective sections below.

I. SYNTHESIS

Synthesis of H_2L^{OMe}

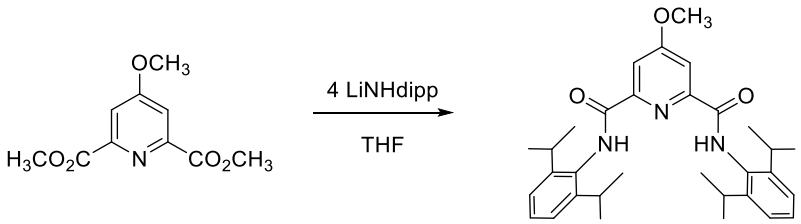

In a glovebox, a 100 mL round-bottom flask was charged with dimethyl 4-methoxypyridine-2,6-dicarboxylate (553 mg, 2.5 mmol, 1 eq) and THF (25 mL); the mixture was stirred until homogeneous. To this stirred solution, LiNHdipp (1.8 g, 9.8 mmol, 3.9 eq) was added over the course of 10 min, forming an orange-hued homogeneous reaction mixture which was allowed to stir for 12h. After this time, the reaction was removed from the glovebox and quenched with dropwise addition of sat. aq. NH_4Cl (30 mL). The resulting mixture was extracted with CH_2Cl_2 (3 x 30 mL); the pooled organic fractions were then washed with H_2O (1 x 30 mL), brine (1 x 30 mL), dried over $MgSO_4$, and dried *in vacuo* to yield a yellow oil. Trituration with hexanes (2 x 30 mL) yielded crude material as an off-white powder. The crude material was further purified via chromatography (silica, 75:25 Hexanes:EtOAc) to furnish H_2L^{OMe} (842 mg, 1.63 mmol, 65%) as a white powder. ^{1}H NMR (500 MHz, $CDCl_3$): δ (ppm) 9.05 (s, 2H, -NH), 8.04 (s, 2H, 3,5-py -CH), 7.36 (t, J = 7.7 Hz, 2H, arm arene *p*-CH), 7.24 (d, J = 7.8 Hz, 4H, arm arene *m*-CH), 4.05 (s, 3H, Py *p*-CH_3), 3.14 (septet, J = 7.0 Hz, 2H, *i*-Pr -CH), 1.23 (d, J = 6.9 Hz, 24H, *i*-Pr 2xCH_3). $^{13}C\{^1H\}$ NMR (126 MHz, $CDCl_3$): δ(ppm) 169.06 (carbonyl), 162.76 (Py, *para*), 150.97 (Py, *ortho*), 146.17 (arm arene, *ortho*), 130.93 (arm arene, *para*), 128.66 (arm arene, *ipso*), 123.73 (arm arene, *meta*), 111.73 (Py, *meta*), 56.37 (*i*-Pr -CH), 29.15 (Py *p*-CH_3), 23.69 (*i*-Pr -CH_3). Anal. calcd (%) for $C_{36}H_{49}N_3O_5$ (as H_2L^{OMe}•EtOAc, 603.80): C, 73.0; H, 8.10; N, 7.51; Found: C, 72.3; H, 8.28; N, 7.17.

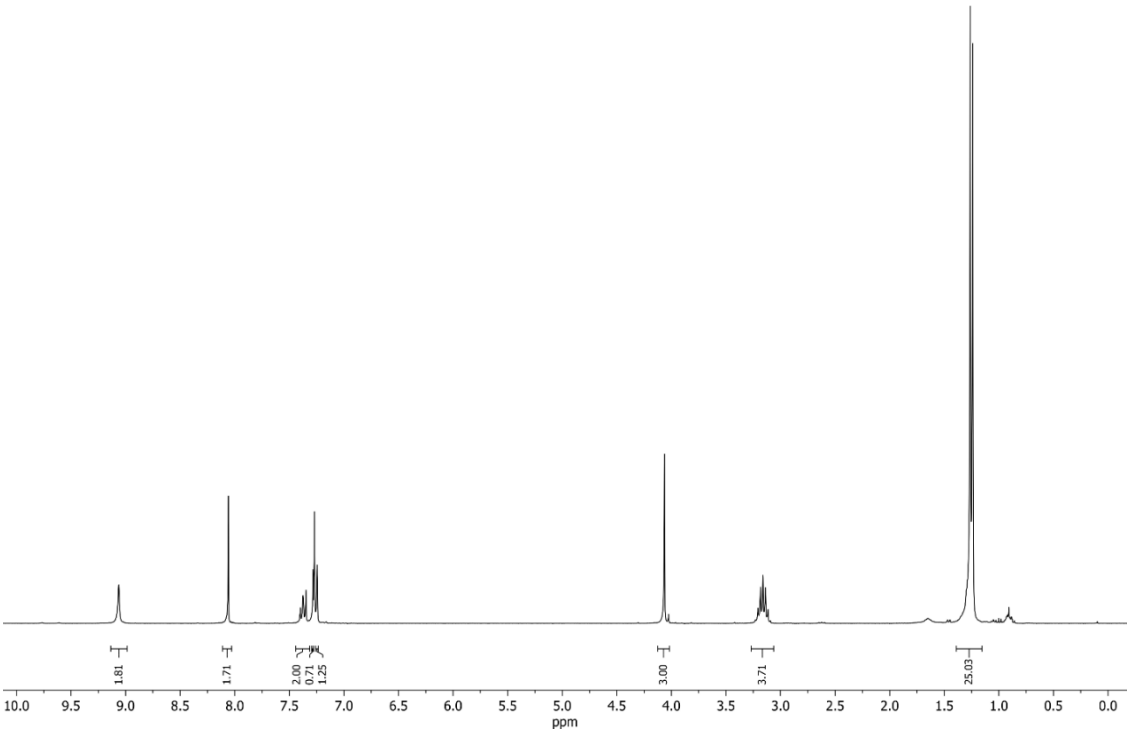

Figure S1. ^{1}H NMR spectrum of H_2L^{OMe} (500 MHz, $CDCl_3$).

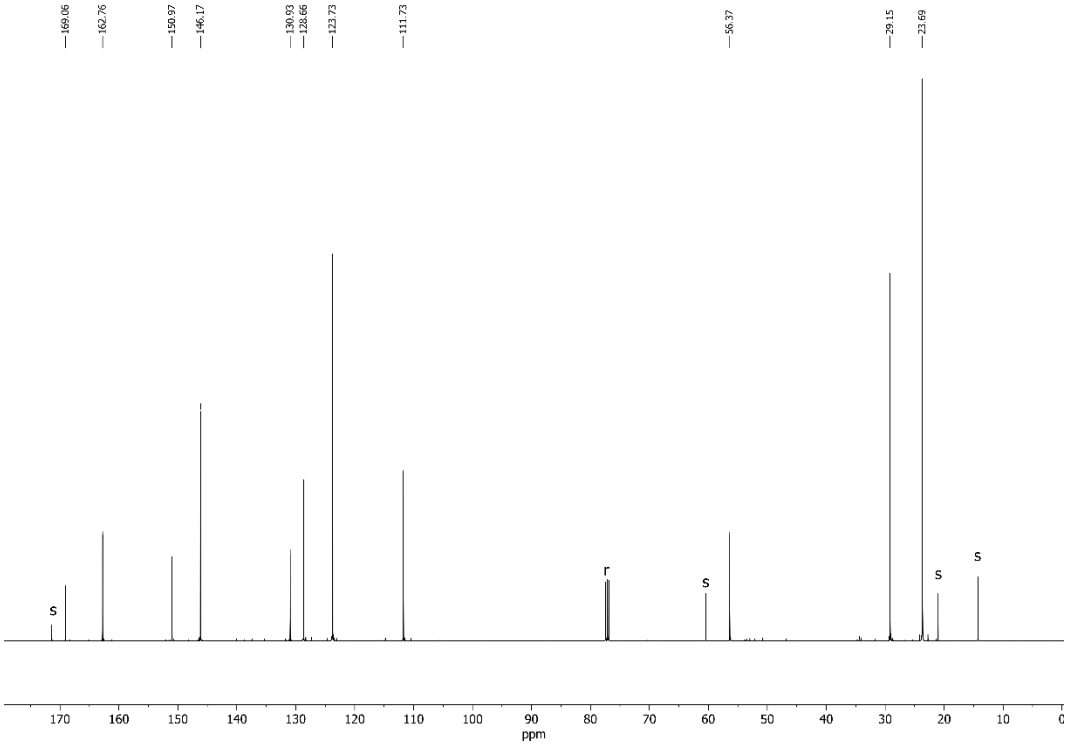

Figure S2. $^{13}C\{^{1}H\}$ NMR spectrum of H_2L^{OMe} (126 MHz, $CDCl_3$). Signals arising from solvent residuals ("r") and traces of ethyl acetate ("s") are indicated.

Synthesis of $L^{OMe}Cu(CH_3CN)$

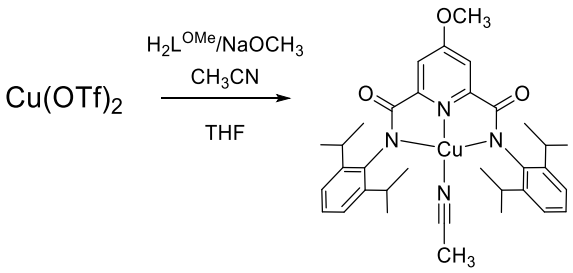

$L^{OMe}Cu(CH_3CN)$

In a glovebox, a 100 mL round-bottom flask was charged with $CuOTf_2$ (420 mg, 1.2 mmol, 1 eq) and H_2L^{OMe} (832 mg, 1.7 mmol, 1 eq). The reagents were then stirred in THF (40 mL), forming a homogeneous solution with a light green tint. Then NaOMe (0.5 M in MeOH, 6.3 mL, 3.2 mmol, 2 eq) was added to the stirred reaction mixture dropwise over 5 min (a rapid color change to dark green was observed during this addition) and allowed to stir for 12 h. The reaction mixture was then exhaustively dried *in vacuo*, yielding a deep green residue. The residue was dissolved in 40 mL of CH_3CN to yield a mahogany solution; the solvent was then removed in vacuo to yield a purple residue. Treatment with CH_3CN and subsequent solvent removal was repeated a total of 3x to ensure complete THF removal. The resulting purple residue was then dissolved in 40 mL of alumina-treated CH_2Cl_2,[8] stirred for 20 min, filtered over Celite to remove NaOTf, and dried *in vacuo* to yield crude $L^{OMe}Cu(CH_3CN)$ as a mahogany solid. Selective precipitation using CH_3CN/Et_2O/pentane yielded purified product (811 mg, 1.30 mmol, 77%) Crystals suitable for X-ray diffraction were obtained by vapor diffusion using CH_2Cl_2/heptane. UV-Vis (CH_3CN, RT): $\lambda_{max}(\varepsilon)$ 325(4450), 402(2850), 539(630). Anal. calcd (%) for $C_{34}H_{42}CuN_4O_3$ (618.28): C, 66.05; H, 6.85; N, 9.06; Found: C, 66.10; H, 6.94; N, 8.72.

Synthesis of [NBu$_4$][Cu(L^{OMe})(OH)]

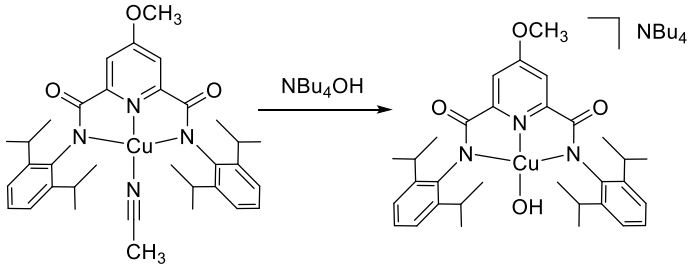

In a glovebox, a 100 mL round-bottom flask was charged with L^{OMe}Cu(CH$_3$CN) (250 mg, 0.40 mmol, 1 eq) and dissolved in THF (30 mL). NBu$_4$OH (1M in MeOH, 0.40 mL, 0.40 mmol, 1 eq) was added dropwise to the stirred reaction mixture, causing the immediate formation of a dark blue solution. The mixture was stirred for 12 h and then dried under dynamic vacuum. The residue was then dissolved in a minimal amount of THF (~2 mL) and precipitated via dropwise addition of Et$_2$O. The mother liquor was decanted, and the process repeated two more times. The resulting material was dried exhaustively *in vacuo* yielding [NBu$_4$][L^{OMe}CuOH] (246 mg, 0.30 mmol, 76%) as a deep blue solid. UV-Vis (THF, -80 °C): λ_{max}(ε) 307(10500), 385(1350), 605(357). Anal. calcd (%) for C$_{48}$H$_{76}$CuN$_4$O$_4$ (836.71) : C, 68.90; H, 9.16; N, 6.70; Found: C, 68.73; H, 9.18; N, 6.56.

Synthesis of [NBu$_4$][L^{H}CuOCH$_2$CF$_3$]

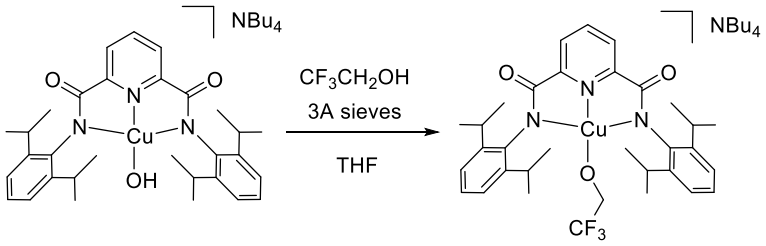

[NBu$_4$][L^{H}CuOH] **[NBu$_4$][L^{H}CuOCH$_2$CF$_3$]**

In a scintillation vial, [NBu$_4$][L^{H}CuOH] (105.2 mg, 0.130 mmol) was dissolved in THF (5.0 mL) followed by addition of 3 Å molecular sieves. To the blue mixture, 2,2,2-trifluoroethanol (47.5 μL, 0.652 mmols, 5 equiv.) was added, and the now dark blue mixture was stirred for 3 h. The solution was then filtered via a syringe PTFE filter, and the solvent was removed, yielding a dark blue oil which was stirred in pentane (5 mL) overnight. The resulting navy blue powder was isolated by decantation, and dried *in vacuo* to give [NBu$_4$][L^{H}CuOCH$_2$CF$_3$] (106.5 mg, 92% yield). X-ray quality crystals were obtained by layering pentane on a concentrated THF solution of the complex. UV-vis (THF) λ_{max}, nm (ε, M^{-1} cm^{-1}): 266 (17000), 302 (*sh*, 12900), 370 (*sh*, 2650), 566 (320), 659 (360). Anal. calcd (%) for $C_{49}H_{75}CuF_3N_4O_3$ (888.71): C, 66.22; H, 8.51; N, 6.30. Found: C, 66.00; H, 8.22; N, 6.19.

Synthesis of [NBu$_4$][L^{OMe}CuOCH$_2$CF$_3$]

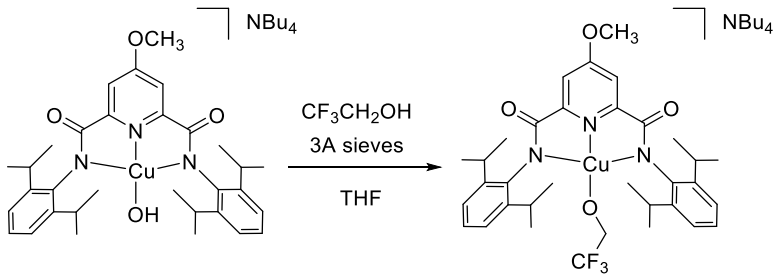

[NBu$_4$][L^{OMe}CuOH] **[NBu$_4$][L^{OMe}CuOCH$_2$CF$_3$]**

In a scintillation vial, [NBu$_4$][L^{OMe}CuOH] (83.6 mg, 0.100 mmol) was dissolved in THF (ca. 3 mL) followed by addition of 3 Å molecular sieves (ca. 300 mg). To the indigo mixture, excess 2,2,2-trifluoroethanol (50 μL, 0.69 mmol) was added, and the now teal-blue mixture was stirred for 2 h. The solution was then filtered by a syringe PTFE filter, and the bulk of the product was precipitated by addition of ca. 5 mL of Et$_2$O and 10 mL of pentane, yielding a dark blue viscous residue and a light blue supernatant. The residue was redissolved in ca. 2 mL THF and layered with ca. 15 mL pentane, then left undisturbed overnight. The product formed blue crystal masses which were decanted and dried *in vacuo* overnight, yielding [NBu$_4$][L^{OMe}CuOCH$_2$CF$_3$] as a blue powder (66.4 mg, 72%). The crystals formed during isolation were not usable for x-ray characterization as even brief exposure outside of the mother liquor resulted in crazing and eventual disintegration, presumably due to loss of volatile solvents of crystallization. Instead, x-ray quality crystals were obtained by storing the initial supernatant solution at -30 °C for 3 days, resulting in a structure incorporating one THF and one 2,2,2-trifluoroethanol molecule per [NBu$_4$][L^{OMe}CuOCH$_2$CF$_3$] moiety. UV-vis (THF) λ_{max}, nm (ε, M^{-1} cm^{-1}): 571 (346), 661 (416). Anal. calcd (%) for C$_{50}$H$_{77}$CuF$_3$N$_4$O$_4$ (918.73): C, 65.37; H, 8.45; N, 6.10. Found: C, 65.54; H, 8.48; N, 5.99.

II. UV-VISIBLE SPECTRA FOR CU(II) COMPLEXES

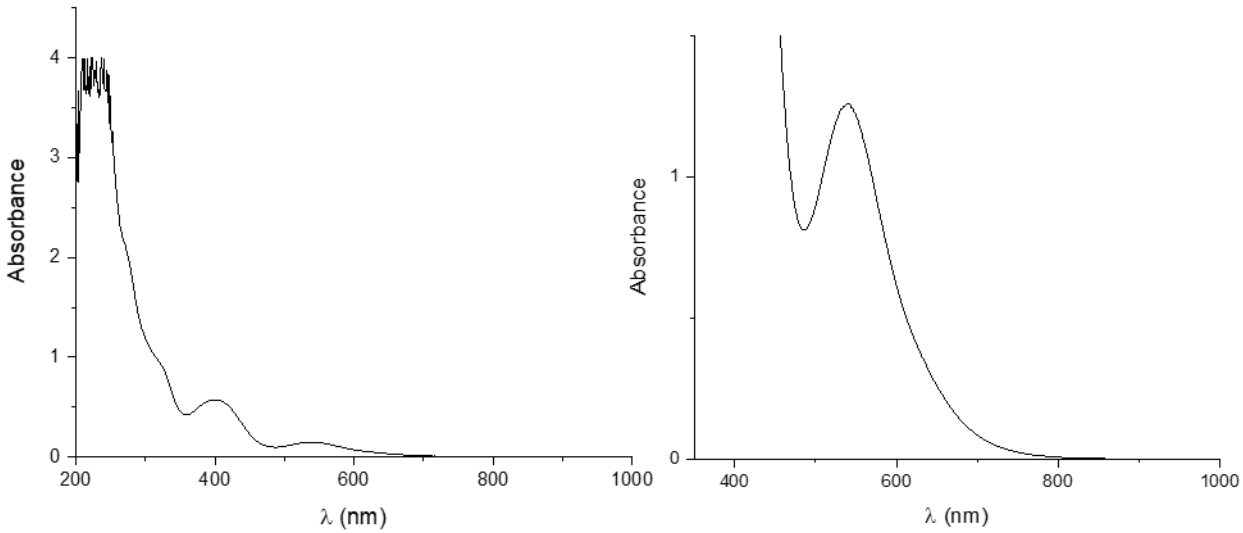

Figure S3. Electronic absorption spectrum of LOMeCu(CH_3CN) in CH_3CN at room temperature. [Cu]: 0.2 mM (left), 2 mM (right).

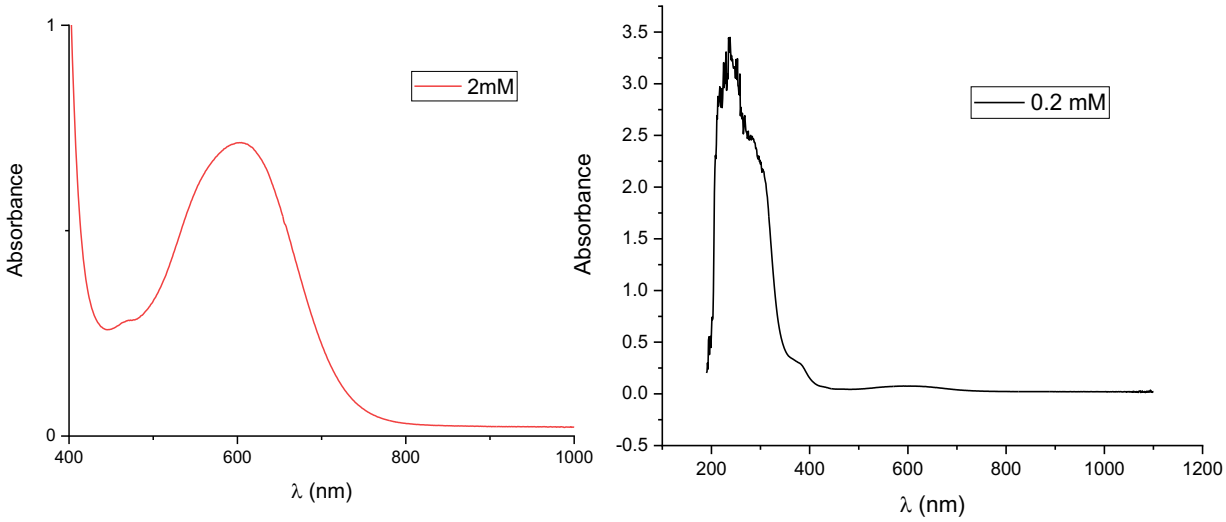

Figure S4. Electronic absorption spectrum of [NBu4][L^{OMe}CuOH] in THF at -80 °C. [Cu]: 0.2 mM (left), 2 mM (right).

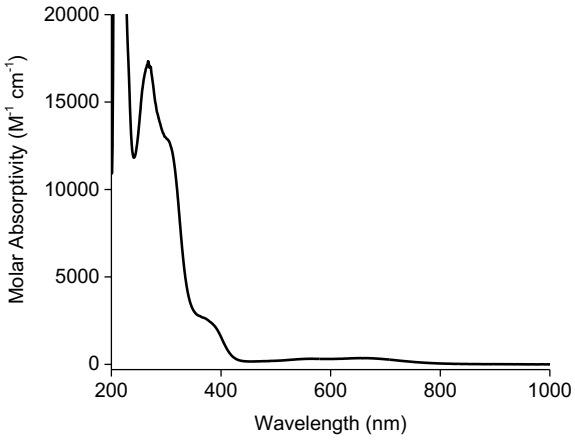

Figure S5. UV-vis spectrum of [NBu_4][$L^{H}CuOCH_2CF_3$]. Conditions: [Cu] = 1.3 mM, THF, -80 °C.

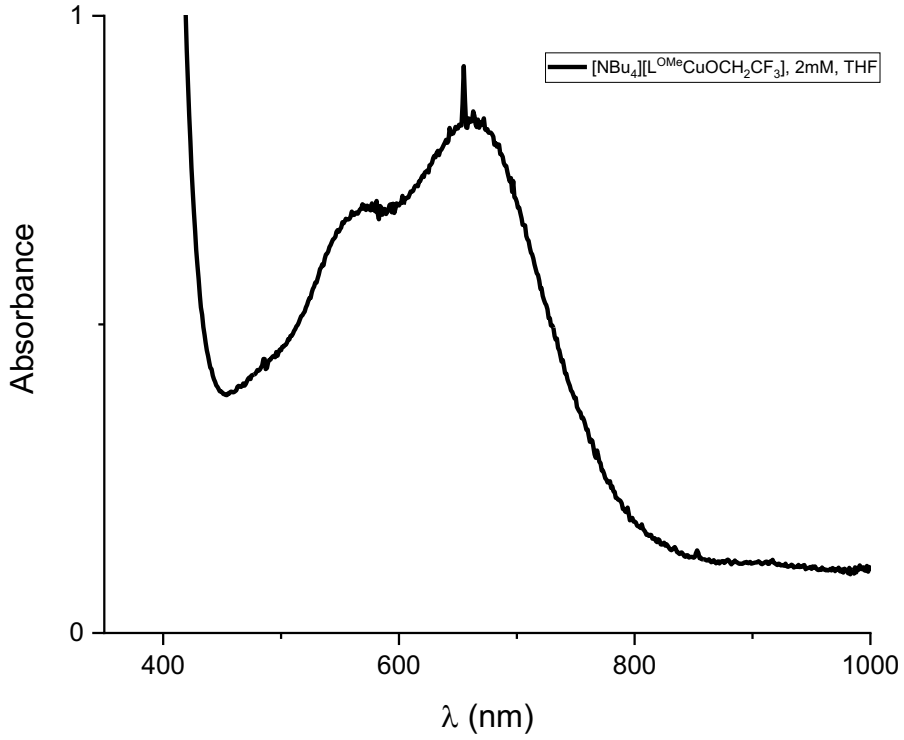

Figure S6. Electronic absorption spectrum of [NBu_4][$L^{OMe}CuOCH_2CF_3$], 2 mM, THF, RT.

III. EPR SPECTROSCOPY

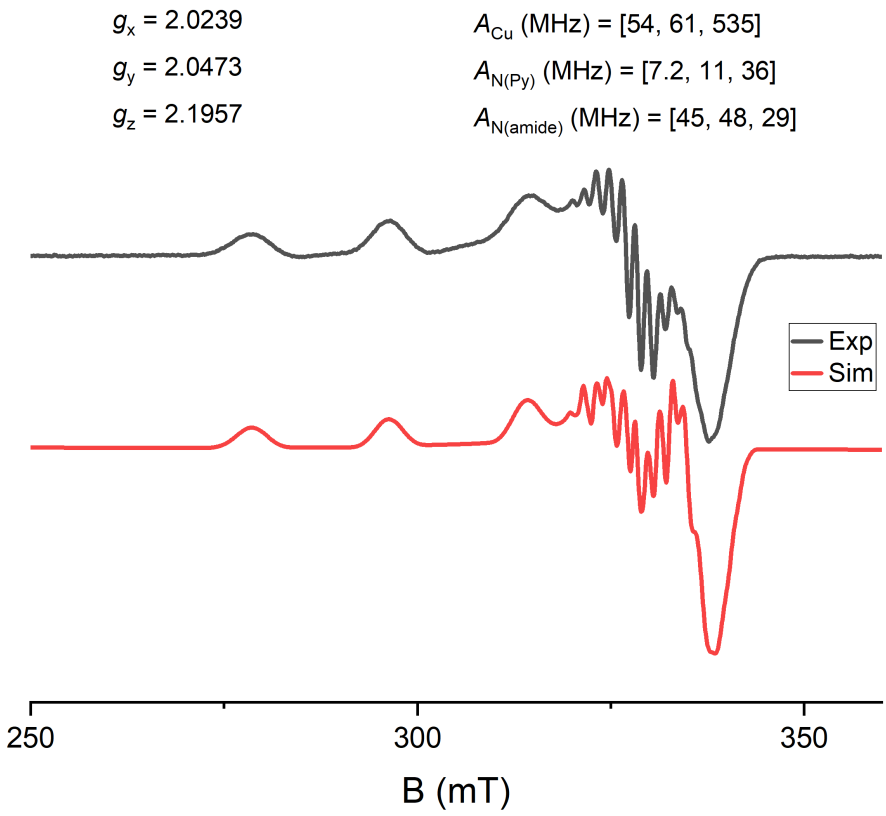

Figure S7. Experimental (black) and simulated (red) X-band EPR spectra of [NBu_4][L^{OMe}CuOH] (1 mM, THF, 0.0635 mW, 30K). Relevant simulated values are as shown.

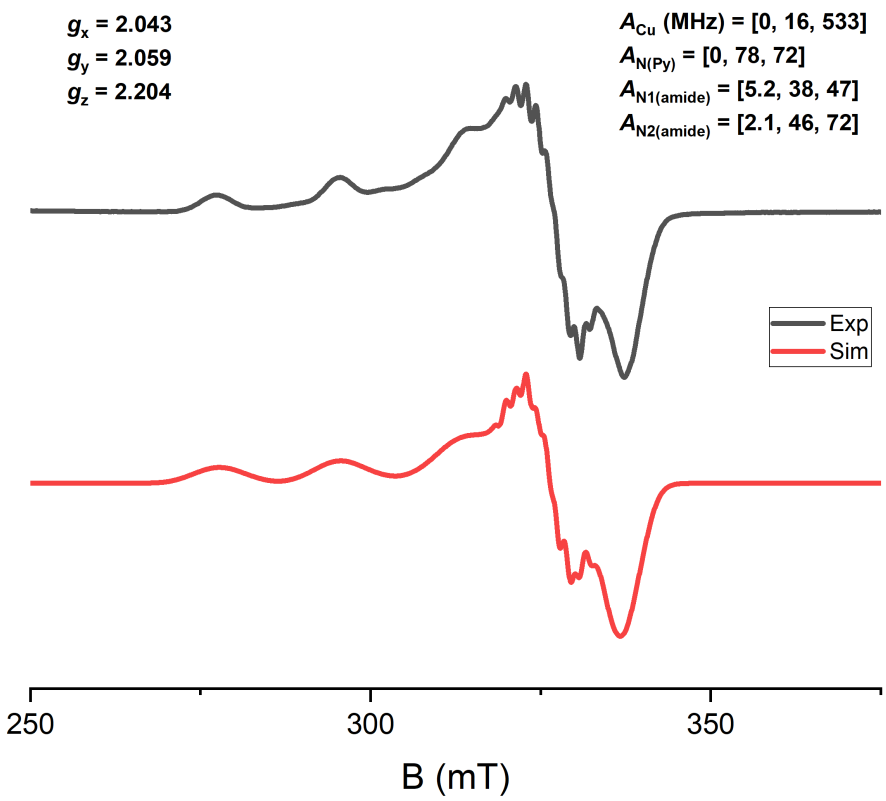

Figure S8. Experimental (black) and simulated (red) X-band EPR spectra of [NBu_4][$L^HCuOCH_2CF_3$] (1 mM, THF, 0.0635 mW, 30K). Relevant simulation parameters are shown.

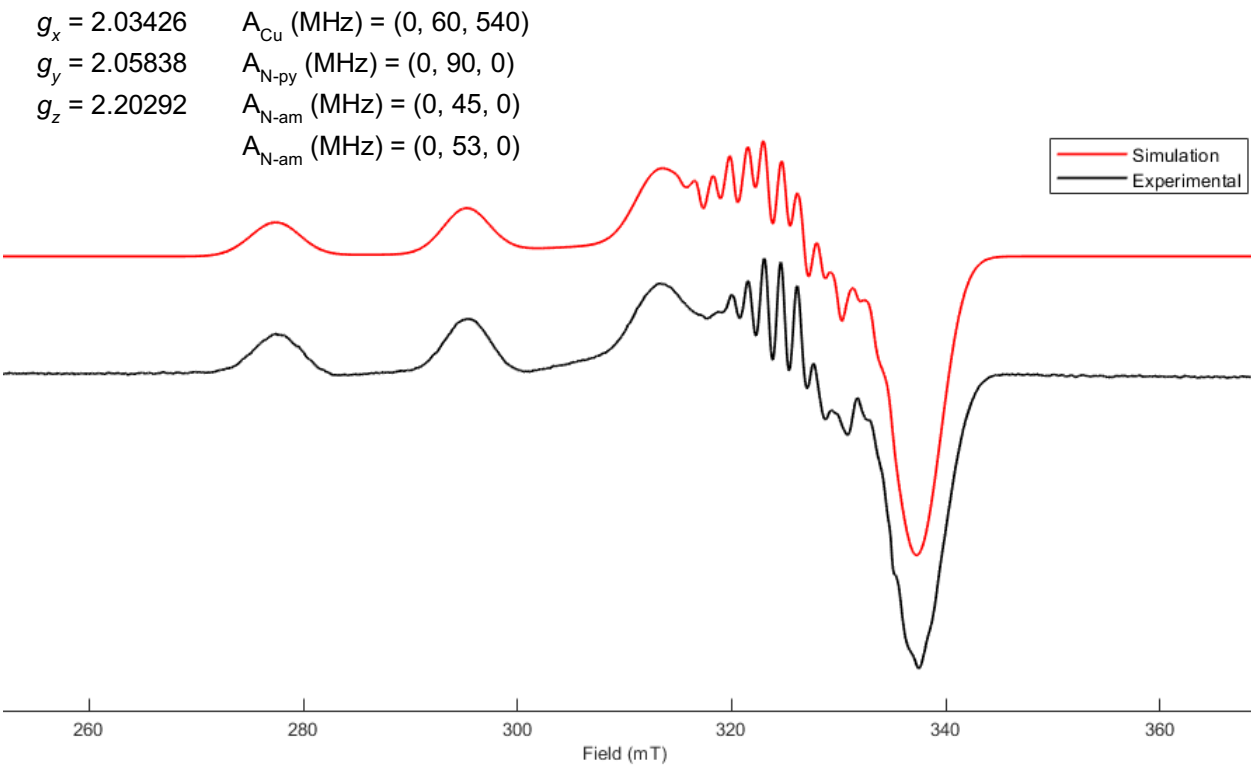

Figure S9. X-band EPR spectrum of [NBu_4][$L^{OMe}CuOCH_2CF_3$] (1 mM, THF, 0.0635 mW, 30K), black, and simulation, red. Relevant simulated values are as shown.

IV. CYCLIC VOLTAMMETRY

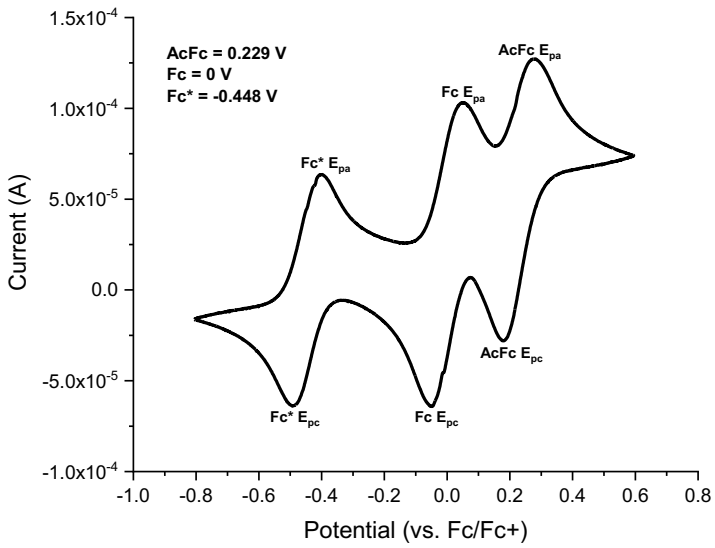

Figure S10. Cyclic voltammogram of decamethylferrocene (Fc*), ferrocene (Fc), and acetylferrocene (AcFc) in THF, 0.2 M NBu_4PF_6, 50 mV s^{-1}. All electrochemical measurements are internally referenced using the $E_{1/2}$ values listed (top left of plot).

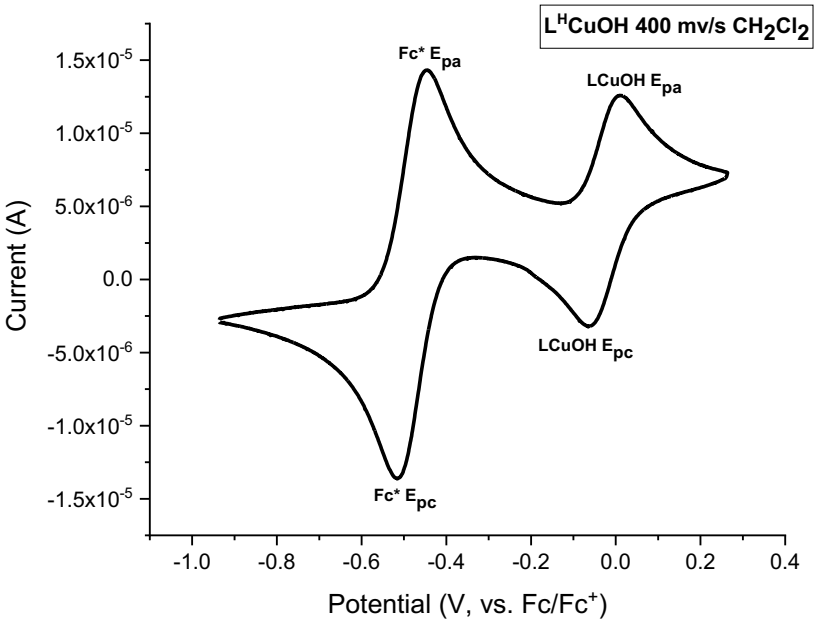

Figure S11. Cyclic voltammogram of [NBu_4][LCuOH] (1 mM, 0.2M NBu_4PF_6, 400 mV/s) in CH_2Cl_2, with the presence of Fc*. Peaks assigned to compound and internal standard are labeled.

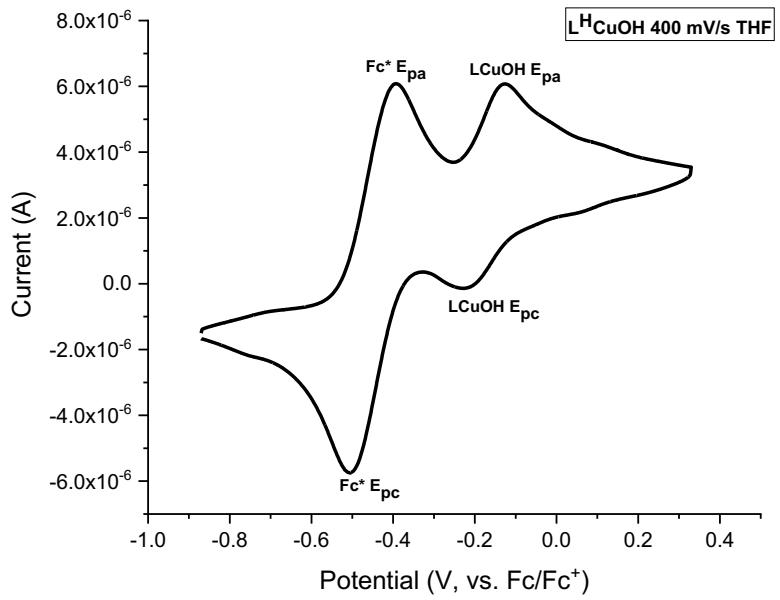

Figure S12. Cyclic voltammogram of [NBu_4][LCuOH] (1 mM, 0.2M NBu_4PF_6, 400 mV/s) in THF, with the presence of Fc*. Peaks assigned to compound and internal standard are labeled.

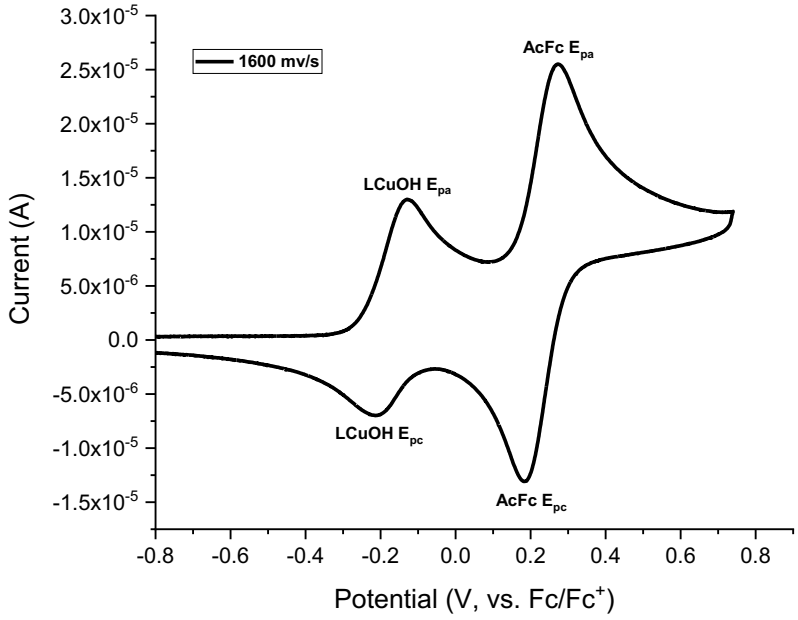

Figure S13. Representative internally-referenced voltammogram of [NBu_4][L^HCuOH] (1 mM, 1600 mV/s, vs. $Fc^{0/+}$) in THF; peaks assigned to AcFc and complex are labeled.

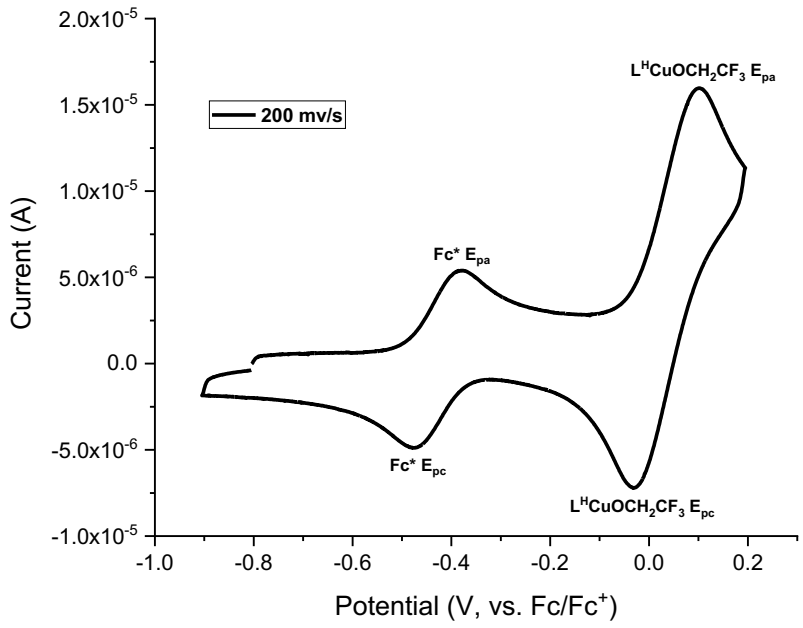

Figure S14. Representative internally-referenced voltammogram of $[NBu_4][L^{H}CuOCH_2CF_3]$ (1 mM, 200 mV/s, vs. $Fc^{0/+}$) in THF; peaks assigned to Fc* and complex are labeled.

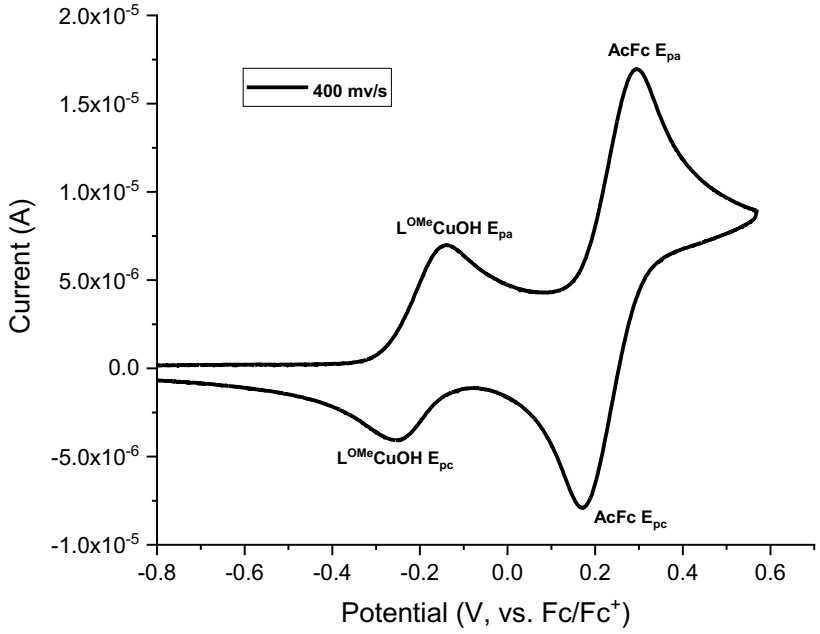

Figure S15. Representative internally-referenced voltammogram of $[NBu_4][L^{OMe}CuOH]$ (1 mM, 400 mV/s, vs. $Fc^{0/+}$) in THF; peaks assigned to AcFc and complex are labeled.

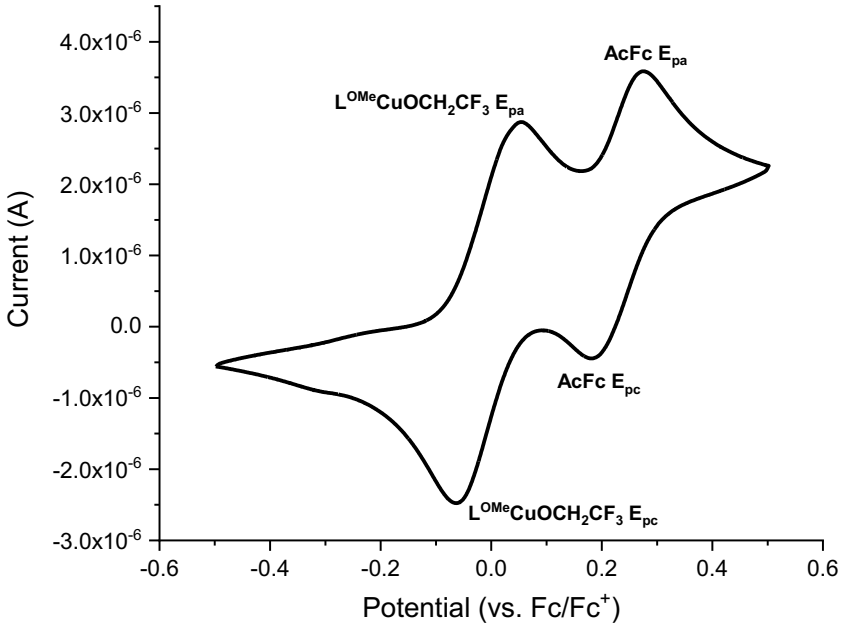

Figure S16. Representative internally-referenced voltammogram of [NBu_4][$L^{OMe}CuOCH_2CF_3$] (1 mM, 200 mV/s, vs. $Fc^{0/+}$) in THF; peaks assigned to AcFc and complex are labeled.

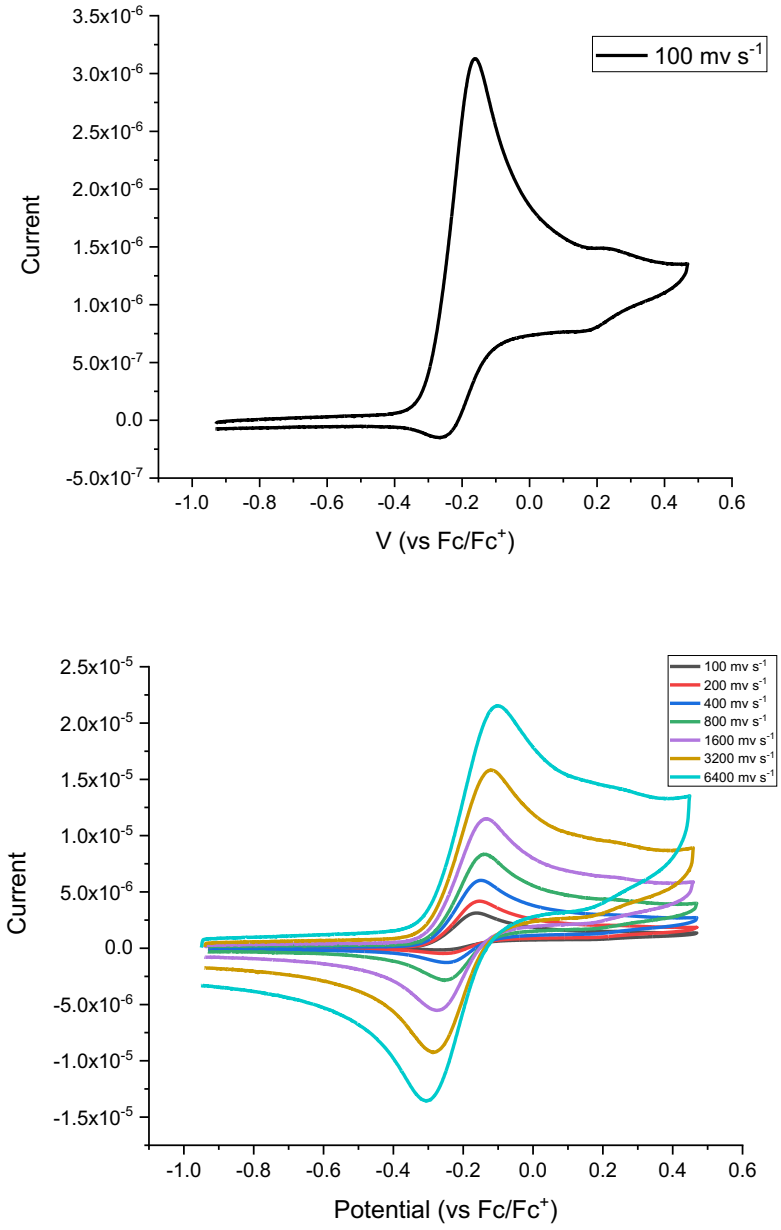

Figure S17. Anodic cyclic voltammetry of $[NBu_4][L^{OMe}CuOH]$ (1 mM) in THF in the presence of NBu_4PF_6 (0.2 M) as electrolyte. TOP: Irreversible anodic voltammogram of $[NBu_4][L^{OMe}CuOH]$ at a scan rate of 100 mV s^{-1} (E_{pa} = -161 mV, i_{pa} = 3.1 µA). BOTTOM: Anodic scans with variable scan rates from 100-6400 mV s^{-1} ($E_{1/2}$ = -202 mV, averaged over scan rates from 400-6400 mV s^{-1}).

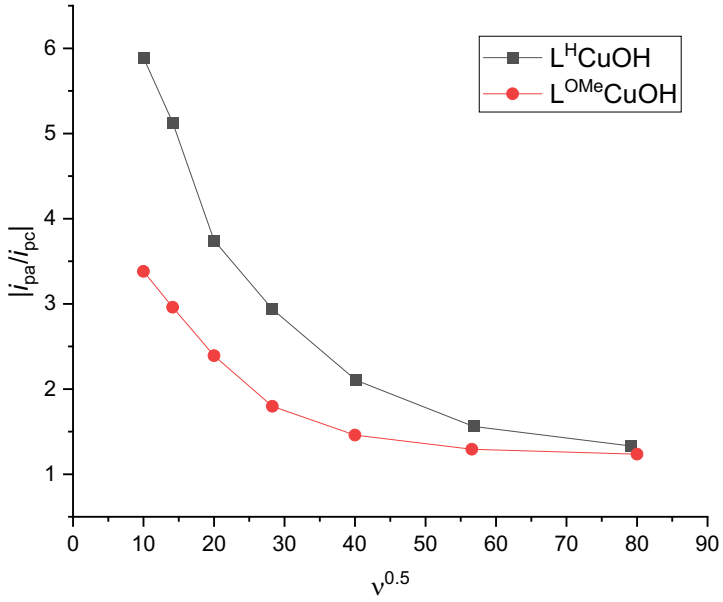

Figure S18. Reversibility comparison of $[CuOH]^{2+}/[CuOH]^{+}$ redox couples of $[NBu_4][L^{H}CuOH]$ vs $[NBu_4][L^{OMe}CuOH]$. Ratio of current intensities of anodic wave and return wave ($|i_{pa}/i_{pc}|$) are plotted as a function of the square root of the scan rate (ν).

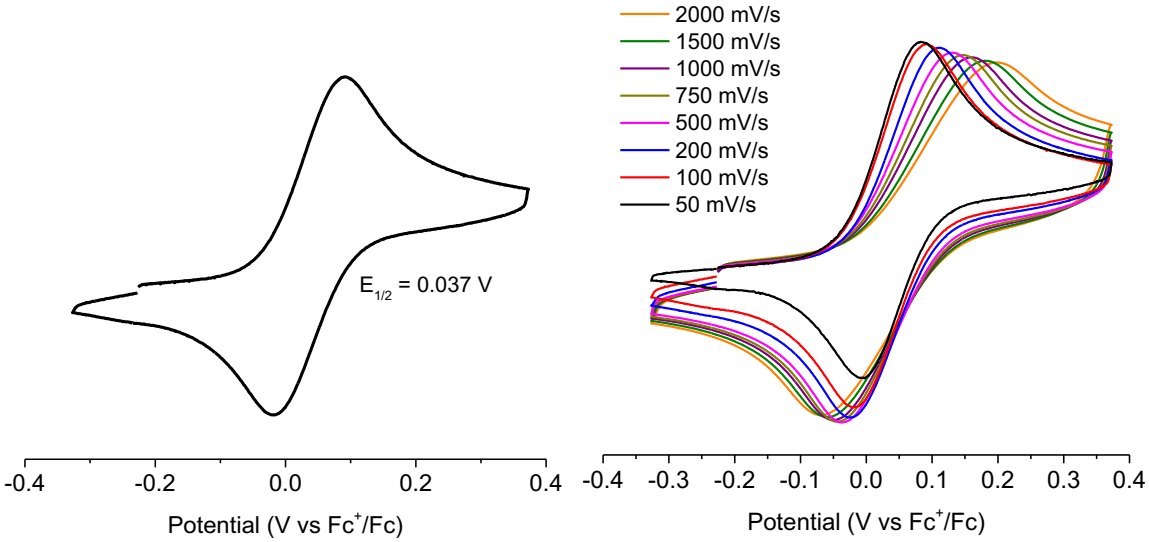

Figure S19. Cyclic voltammograms of $[NBu_4][L^{H}CuOCH_2CF_3]$ at a scan rate of 100 mV/s (left) and scan rate normalized traces at varying scan rates (right). Conditions: [Cu] = 1 mM, THF, $[NBu_4PF_6]$ = 0.2 M.

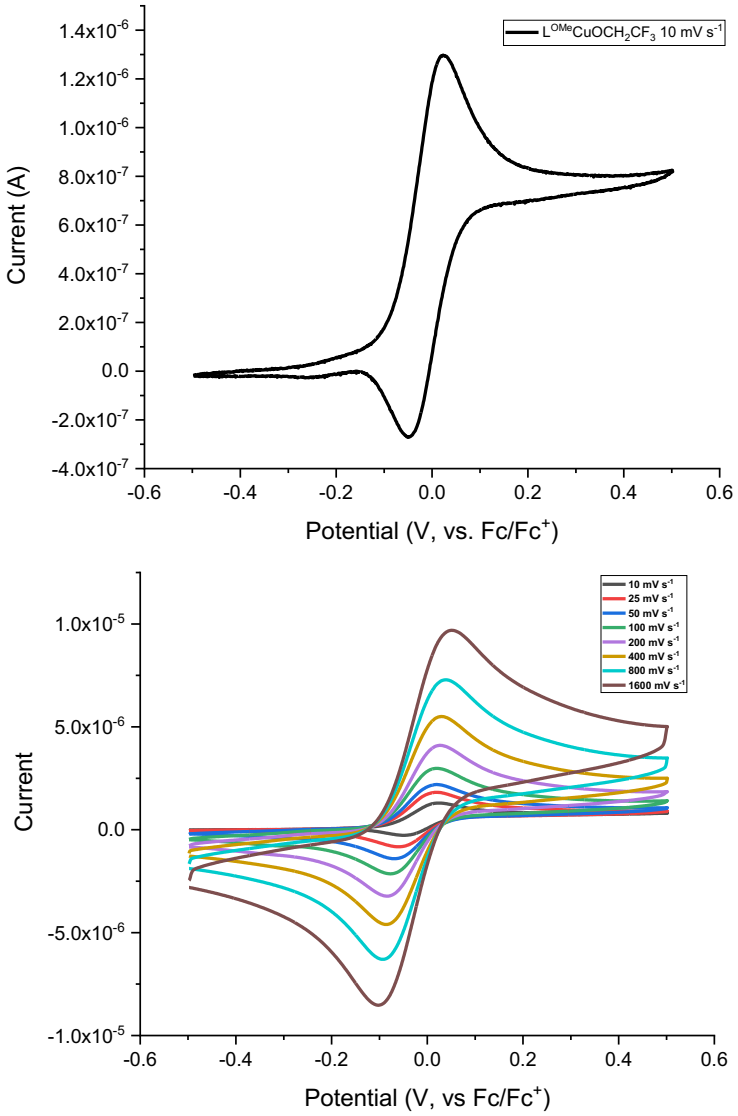

Figure S20. Cyclic voltammograms of $[NBu_4][L^{OMe}CuOCH_2CF_3]$ at a scan rate of 10 mV s^{-1} (top) and traces at varying scan rates (bottom). Conditions: [Cu] = 1 mM, THF, $[NBu_4PF_6]$ = 0.2 M ($E_{1/2}$ = -24 mV, averaged over all experimental scan rates).

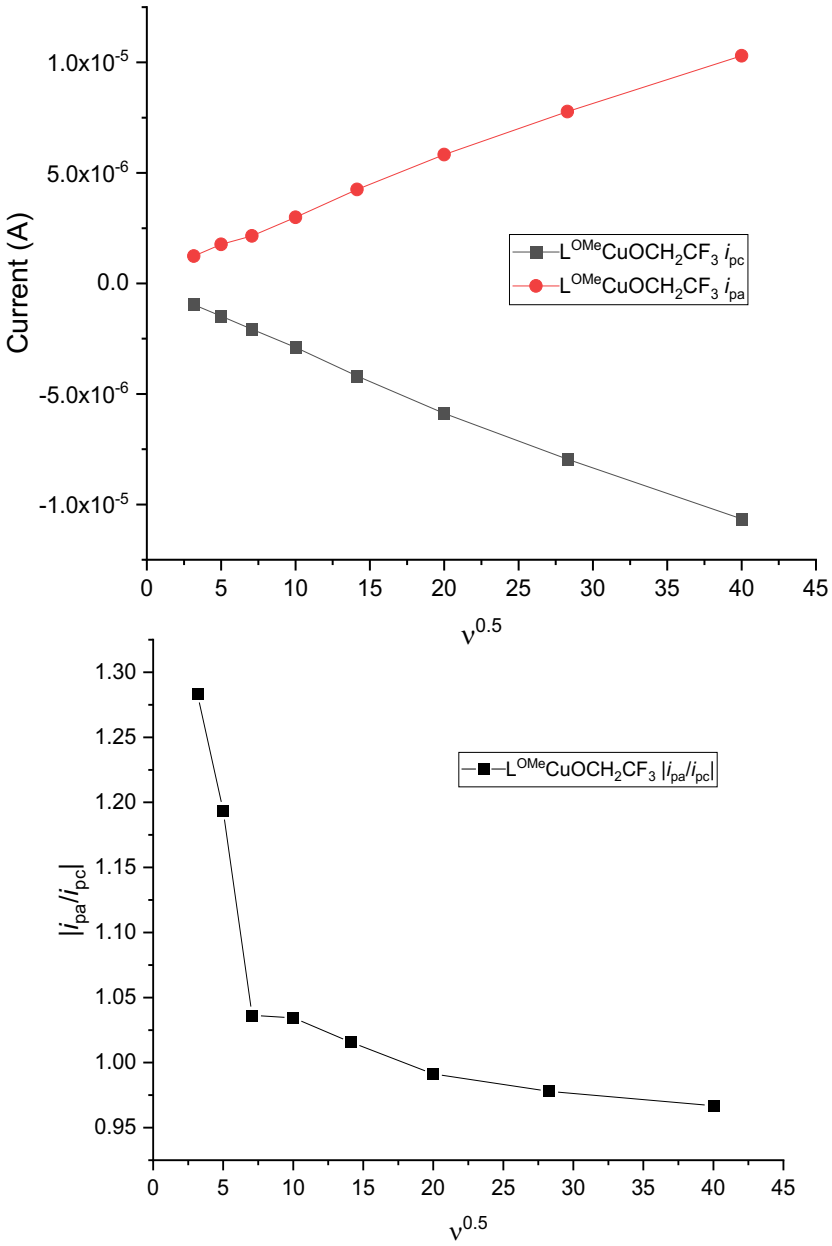

Figure S21. Reversibility of $[CuOR]^{2+}/[CuOR]^{+}$ redox couple of $[NBu_4][L^{OMe}CuOCH_2CF_3]$. TOP: Current response as a function of the square root of the scan rate; BOTTOM: Ratio of current intensities of anodic wave and return wave ($|i_{pa}/i_{pc}|$) are plotted as a function of the square root of the scan rate.

Reduction potential of $L^{H}CuOH$

We note that the $E_{1/2}$ value we presently measure for $[NBu_4][L^{H}CuOH]$ in THF (-0.167 V vs $Fc^{0/+}$) conflicts with a previously reported value (-0.074 V) from our group.[9] However, measurement in CH_2Cl_2 yielded a result in agreement with our previously reported value in that solvent.[10] We believe that our current measurement reflects the true potential of this redox couple in THF, and postulate that this discrepancy may have arisen from the practice of external referencing using the Ag wire pseudo-reference electrode in the previous measurement of this value in THF. External referencing can introduce calibration errors as any changes to the Ag wire surface occurring between measurement of the analyte and reference will offset the reported value. Our current and other previous works report $[NBu_4][L^{H}CuOH]$ potentials internally referenced to ferrocene (Fc) decamethylferrocene (Fc*) or acetylferrocene (AcFc); representative internally-referenced voltammograms are provided for all standards, $[NBu_4][L^{H}CuOH]$, and all novel complexes in this report.

V. CHEMICAL FORMATION OF $L^{Y}CuOR$ SPECIES

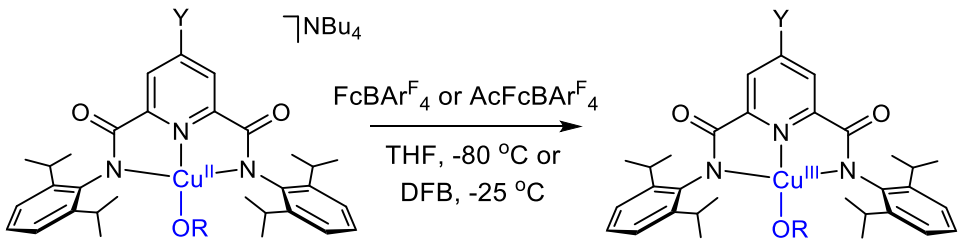

General Procedures

Generation of $L^{Y}CuOR$. Under argon, a cuvette with 1.8 mL of neat solvent (THF or 1,2-fluotobenzene, DFB) was placed inside a Unisoku low temperature cell holder pre-cooled to the specified temperature (−80 °C in THF or −25 °C in DFB) and allowed to thermally equilibrate at least 7 min; a blank spectrum was then recorded. A 0.1 mL aliquot of 2.0 mM $[NBu_4][L^{Y}CuOR]$ in the respective solvent was injected to the sample. To this stirred solution, 0.1 mL of 2.0 mM oxidant solution ($FcBAr^{F}_4$ for OR = OH, $AcFcBAr^{F}_4$ for OR = OCH_2CF_3) was added to the to generate the corresponding $L^{Y}CuOR$ species *in situ*, and a spectrum of the oxidized species was collected approximately 5 seconds after injection of the oxidant. The stoichiometry of the oxidation was established using incremental titration carried out in a similar manner, using a 0.4 mM solution of the corresponding oxidant added 0.1 mL at a time into a solution containing a total of 0.2 μmol of $[NBu_4][L^{Y}CuOR]$ in 1.5 mL (see figures below). In all cases, a 1:1 reaction stoichiometry was observed.

$L^{OMe}CuOH$

Deep purple solution forms. UV-Vis: λ_{max}, nm (ε, M^{-1} cm^{-1}): 542 (13600, THF, -80 °C); 554 (11500, DFB, -25 °C).

$L^{H}CuOCH_2CF_3$

Deep blue solution forms. UV-vis (THF, -80 °C) λ_{max}, nm (ε, M^{-1} cm^{-1}): 420 (*sh*, 4200) 629 (12400), 715 (10900). UV-vis (DFB, -25 °C) λ_{max}, nm (ε, M^{-1} cm^{-1}): 643 (11800), 756 (11300).

$L^{OMe}CuOCH_2CF_3$

Deep blue solution forms. UV-vis (DFB, -25 °C) λ_{max}, nm (ε, M^{-1} cm^{-1}): 461 (*sh*, 5900), 625 (10980), 734 (*sh*,9800). UV-vis (THF, -80°C) λ_{max}, nm (ε, M^{-1} cm^{-1}): 461 (*sh*, 5900), 608 (12050), 730 (*sh*, 9400).

Chemical Reversibility Experiments

In a glovebox, a cuvette containing neat THF was sealed with a rubber septum, removed from the glovebox, and placed in a Unisoku low temperature cell holder pre-cooled to the specified temperature, and put under argon. Once the sample had thermally equilibrated (at least 7 min), a blank spectrum was taken. A 0.1 mL aliquot of 2.0 mM $[NBu_4][L^{Y}CuOR]$ was injected, resulting in the concentration indicated below, and an initial spectrum taken. To this stirred solution, repeated sequential additions of 0.1 mL of 2.0 mM oxidant ($FcBAr^{F}_4$ for -OR = -OH, $AcFcBAr^{F}_4$ for -OR = $-OCH_2CF_3$) and reductant ($FeCp^*_2$) were performed. Reaction progress was monitored by UV-Vis spectroscopy (see below).

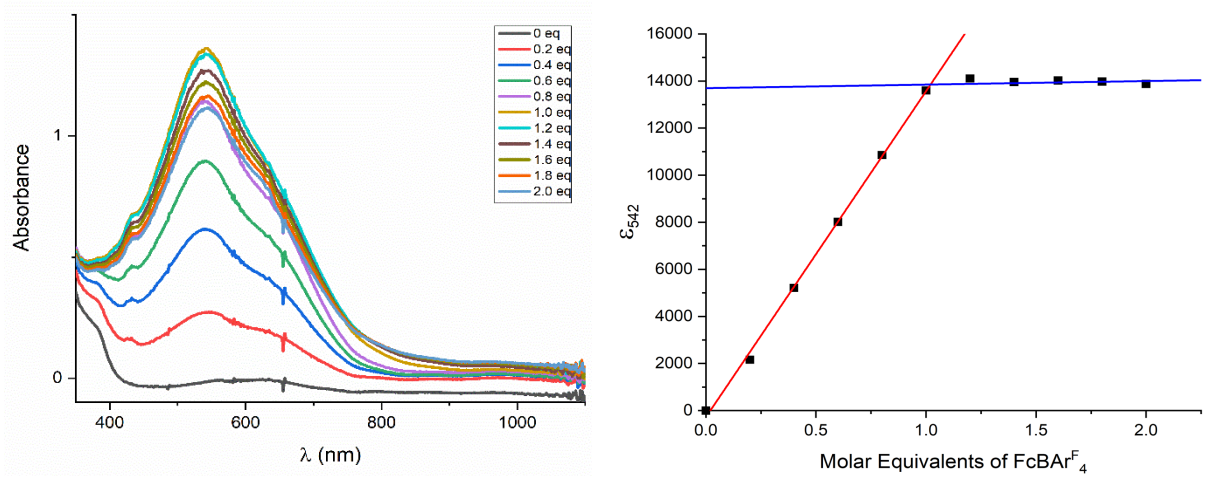

Figure S22. Electronic spectra of $L^{OMe}CuOH$ generated in situ from $[NBu_4][L^{OMe}CuOH]$, THF, -80 °C. LEFT: Titration of $[NBu_4][L^{OMe}CuOH]$ with $FcBAr^F_4$ (0-2 eq); RIGHT: Plot of ε (λ_{max} = 542 nm) with respect to molar eq. of $FcBAr^F_4$.

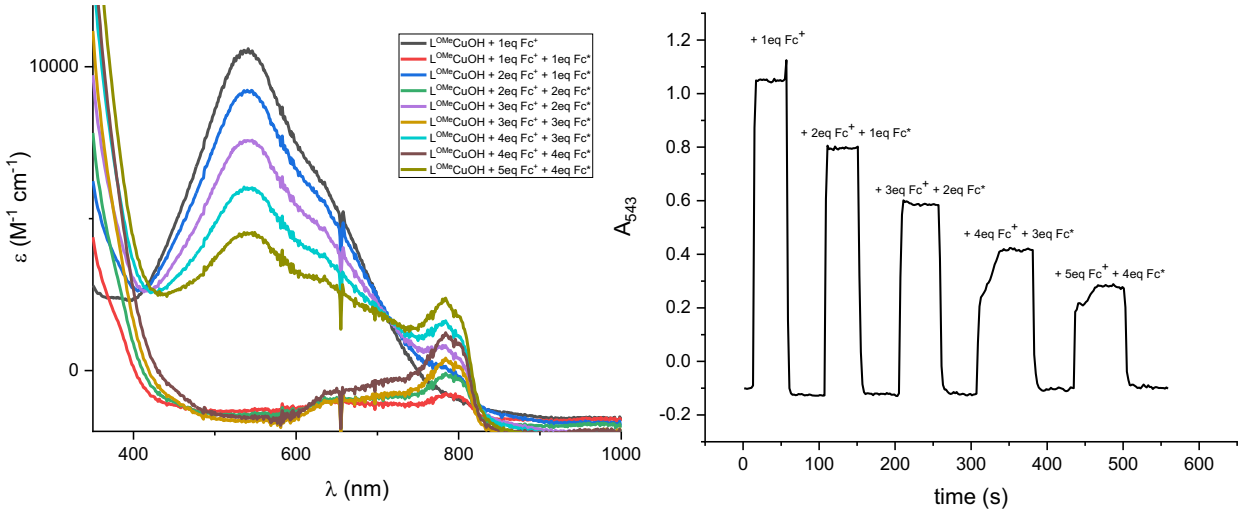

Figure S23. Sequential treatment of $[NBu_4][L^{OMe}CuOH]$ with $FcBAr^F_4$ in THF at -80 °C (generating $L^{OMe}CuOH$) and $Fe(Cp^*)_2$ (regenerating $[NBu_4][L^{OMe}CuOH]$ and $[Fc^*]^+$; $[Cu]_0$ = 0.13 mM.. LEFT: Full spectra after additions as noted; RIGHT: Kinetics trace at λ_{max}= 543 nm; peak plateaus correspond to $L^{OMe}CuOH$, troughs correspond to $[NBu_4][L^{OMe}CuOH]$ and $[Fc^*]^+$.

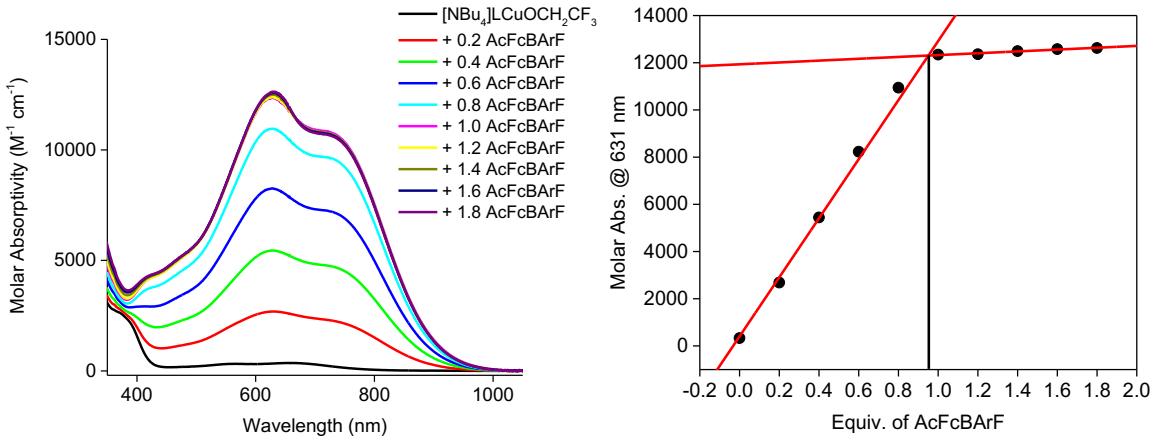

Figure S24. UV-vis spectra stack of the addition of [AcFc][BAr^F_4] (0.2 equiv/aliquot) to [NBu_4][$L^HCuOCH_2CF_3$] (left) and the corresponding molar absorptivity values at λ_{max} 631 nm after each aliquot addition (right). Conditions $[Cu]_0$ = 1.3 mM, THF, -80 °C.

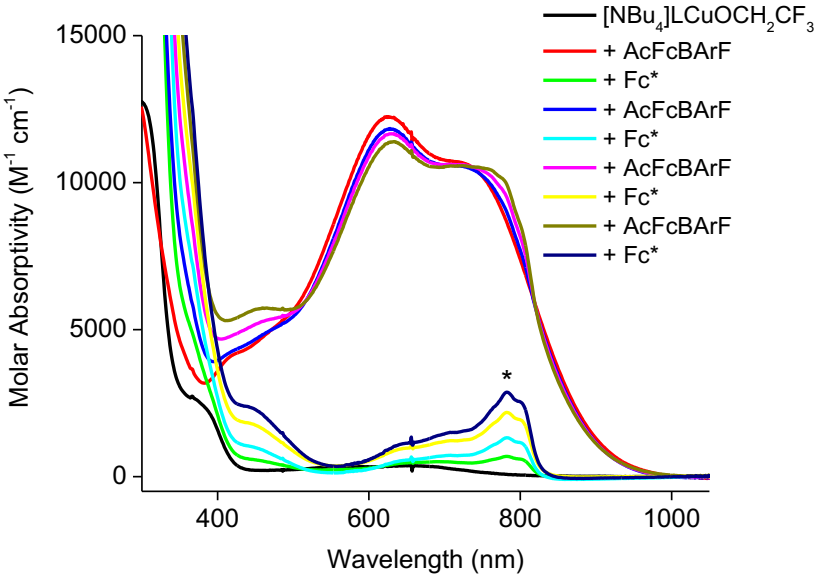

Figure S25. UV-vis spectra of the subsequent additions of [AcFc][BAr^F_4] and Fc* to [NBu_4][$LCuOCH_2CF_3$]. Conditions $[Cu]_0$ = 0.11 mM, THF, -80 °C. (* denotes decamethylferrocenium signal).

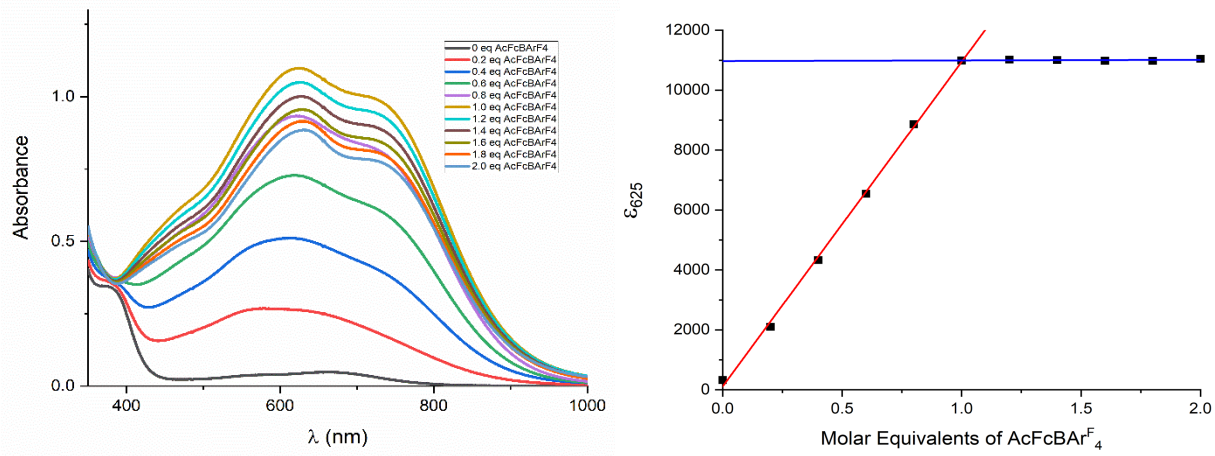

Figure S26. Electronic spectra of $L^{OMe}CuOCH_2CF_3$ generated *in situ* from $NBu_4][L^{OMe}CuOCH_2CF_3]$, DFB, -25°C. LEFT: Titration of $[NBu_4][L^{OMe}CuOCH_2CF_3]$ with $AcFcBAr^F_4$ (0-2eq); RIGHT: Plot of e (λ_{max} = 542 nm) with respect to molar eq. of $AcFcBAr^F_4$.

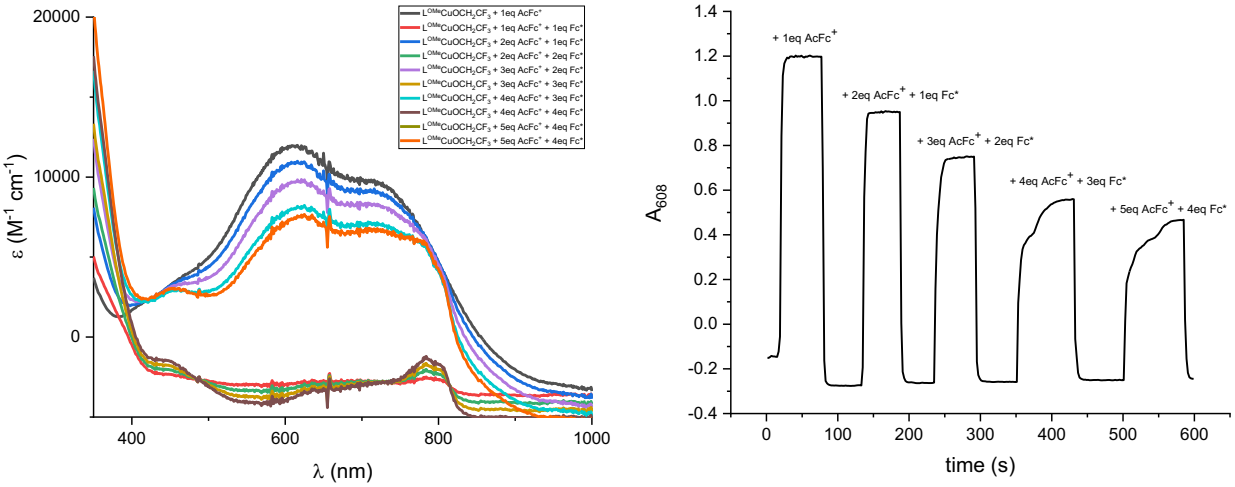

Figure S27. Sequential treatment of $[NBu_4][L^{OMe}CuOCH_2CF_3]$ with $AcFcBAr^F_4$ in THF at -80 °C. (generating $L^{OMe}CuOCH_2CF_3$) and $Fe(Cp^*)_2$ (regenerating $[NBu_4][L^{OMe}CuOCH_2CF_3]$ and $[Fc^*]^+$; $[Cu]_0$ = 0.13 mM. LEFT: Full spectra after additions as noted; RIGHT: Kinetics trace at λ_{max}=604 nm; peak plateaus correspond to $L^{OMe}CuOCH_2CF_3$, troughs correspond to $[NBu_4][L^{OMe}CuOCH_2CF_3]$ and $[Fc^*]^+$.

VI. NMR SPECTROSCOPY OF $L^{Y}CuOR$

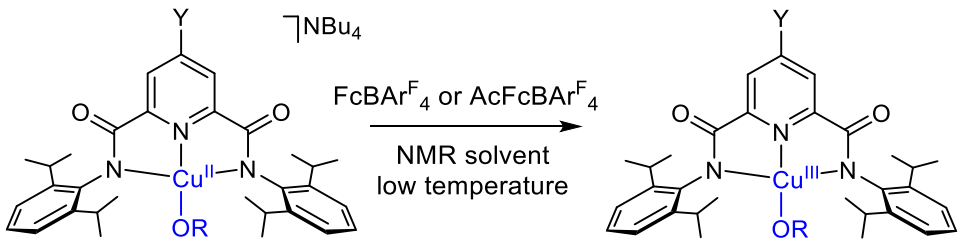

General Procedure

A solution of $[NBu_4][L^{Y}CuOR]$ (Y = -H, -OMe; R = -H, $-OCH_2CF_3$) in the specified NMR solvent was placed in a J Young tube outfitted with a rubber septum and cooled as indicated. To this cooled solution, under Ar flow, a solution of oxidant ($FcBAr^{F}_4$ or $AcFcBAr^{F}_4$) was slowly added via syringe to the tube and allowed to layer. The sample was allowed to thermally equilibrate (~2 min) and then rapidly mixed; the septum was then removed and immediately replaced with a Teflon pin under Ar flow. The tube was then quickly placed inside a pre-cooled spectrometer and the spectrum was acquired. See specific details for each experiment below.

^{1}H NMR Analysis of $L^{Y}CuOH$ (Y = -H, -OMe)

Solutions of $[NBu_4][L^{Y}CuOH]$ (4.0 mg, Y = H; 4.2 mg, Y = OMe), in DCB-d_4 (0.5 mL, dried over 3Å sieves), $FcBAr^{F}_4$ (1.0 mL, 5 mM, in DCB-d_4) were prepared and handled as described in the General Procedure using a saturated NaCl-ice cooling bath (−20 °C) and a spectrometer pre-cooled to -15 °C (Figure S28). ^{1}H NMR (Y = OMe, 500 MHz, DCB-d_4, -15 °C): δ (ppm) 1.34 (24H, 4xCH_3, -iPr), 3.42 (3H, *p*-OCH_3), 3.70 (4H, iPr -CH), 4.22 (1H, -OH), 6.88 (2H, aryl), 7.1 (4H, aryl), 7.29 (2H, aryl). For Y=-OMe, after the initial acquisition, the sample removed from the spectrometer and exposed to room temperature for ca. 1 minute then replaced in the instrument and remeasured; the recorded spectrum suffered from a loss in resolution and showed spectral quality comparable to that obtained for $L^{H}CuOH$ (Figure S29).

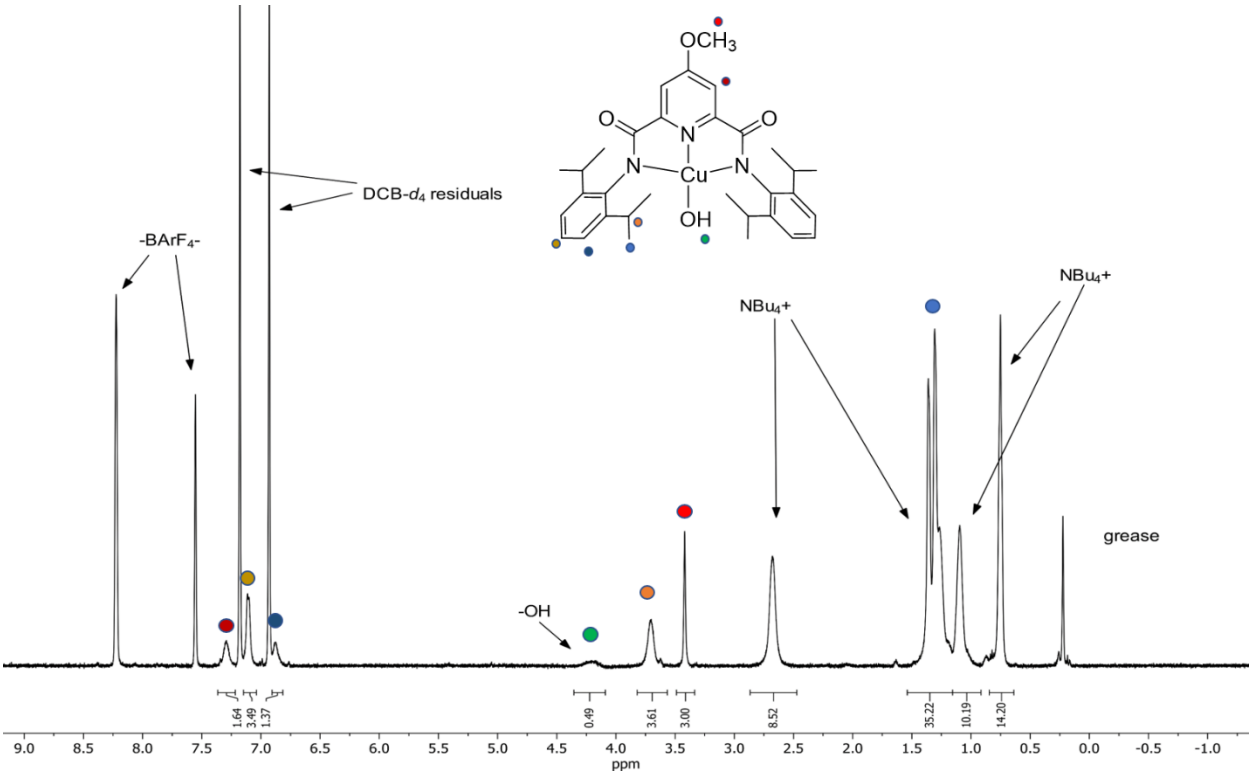

Figure S28. ^{1}H NMR spectrum of $L^{OMe}CuOH$ at -15 °C. Resonances corresponding to solvent residuals and $NBu_4BAr^F{}_4$ are indicated.

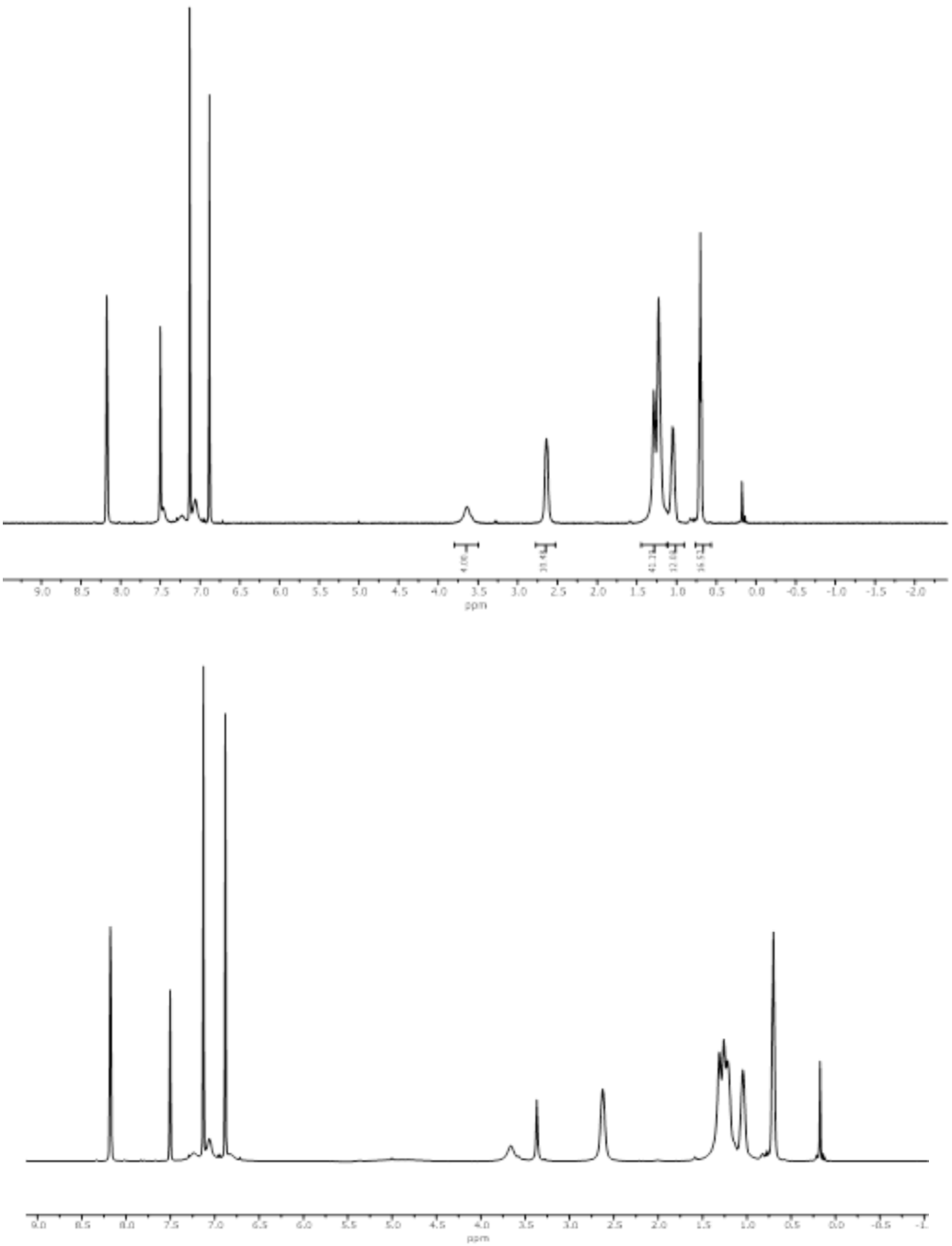

Figure S29.TOP: ^{1}H NMR spectrum of L^{H}CuOH immediately after generation; BOTTOM: ^{1}H NMR spectrum of L^{OMe}CuOH after exposure to room temperature.

^{1}H NMR Analysis of $L^HCuOCH_2CF_3$

Following the General Procedure, a solution of $[NBu_4][L^HCuOCH_2CF_3]$ (4.5 mg, 5.1 mmol) in THF-d_8 (0.4 mL) was treated with $[AcFc][BAr^F{}_4]$ (5.5 mg in 0.4 mL THF-d_8) in an acetone/dry-ice bath, then quickly added to a precooled NMR spectrometer (-80 °C) for acquisition. ^{1}H NMR (300 MHz, THF-d_8) δ (ppm) 1.10 (d, J^3_{HH} = 5.6 Hz, 12H, -CH_3), 1.22 (d, J^3_{HH} = 6.0 Hz, 12H, -CH_3), 2.20 (q, J^3_{HF} = 9.1 Hz, 2H, -CH_2-CF_3), 7.13 (d, J^3_{HH} = 7.6 Hz, 4H, Ar-H), 7.38 (t, J = 7.7 Hz, 2H, Ar-H), 8.15 (br, 2H, Py-H), 8.58 (br, 1H, Py-H). The isopropyl methylene C-H signal was overlapped by THF residual signal. The $[NBu_4][BAr^F{}_4]$ salt and AcFc signals were identified from independent NMR samples.

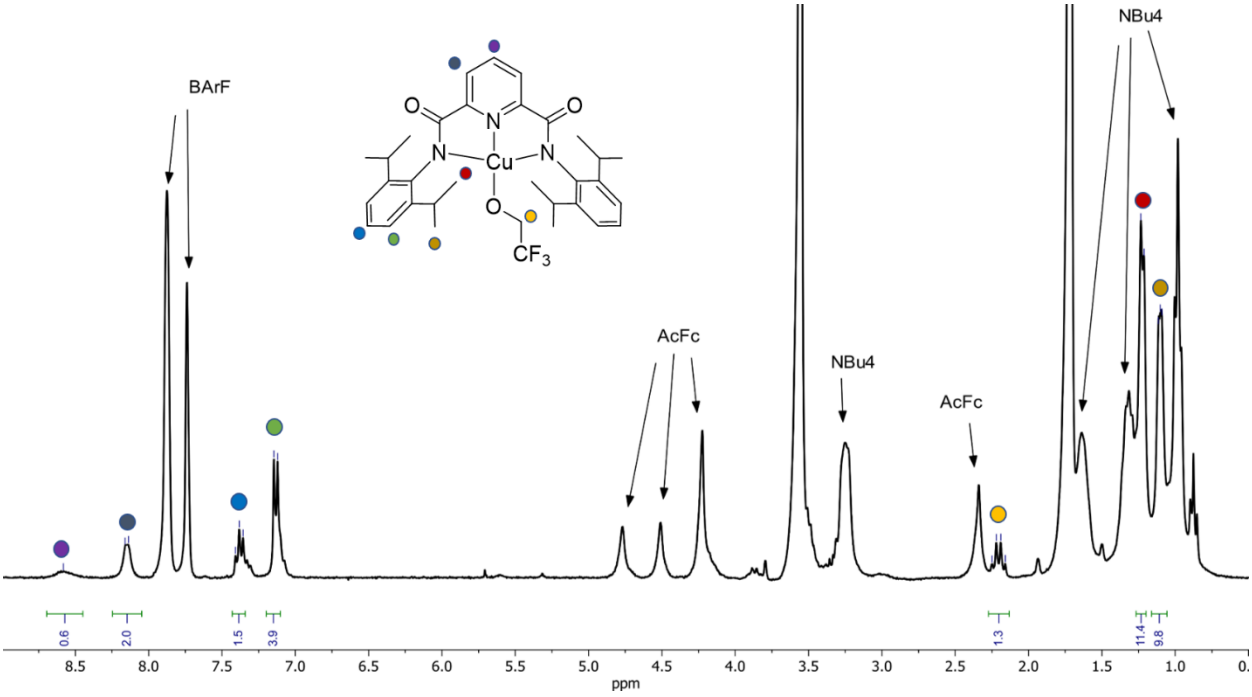

Figure S30. ^{1}H NMR spectrum of the reaction of $L^HCuOCH_2CF_3$ (300 MHz, THF-d_8 , -80 °C). Resonances corresponding to $[NBu_4][BAr^F{}_4]$ and AcFc are annotated.

^{1}H NMR Analysis of $L^{OMe}CuOCH_2CF_3$

^{1}H and ^{13}C{1H} NMR spectra were acquired using the General Procedure with the following modifications: isolated **$L^{OMe}CuOCH_2CF_3$** (4.4 mg) prepared as described for crystallization (see section IX below) was placed in a J. Young tube and cooled to -20 °C in a salt-water ice bath. CD_2Cl_2 (0.5 mL) was subsequently injected and mixed at -20 °C until dissolved. The sample was placed in a pre-cooled spectrometer (-15 °C) and the spectrum immediately acquired. ^{1}H NMR (500 MHz, CD_2Cl_2, -15°C): δ (ppm) 1.13 (d, 12H, J^{3}_{HH}=6.74 Hz, -CH_3 (i-Pr)), 1.21 (d, 12H, J^{3}_{HH} = 6.77 Hz, -CH_3 (i-Pr)), 2.06 (q, 2H, J^{3}_{HF}=9.0 Hz, -CH_2-), 3.30 (septet, 4H, J^{3}_{HH}=6.45 Hz, -CH (i-Pr)), 4.12 (s, 3H, *p*-OCH_3), 7.12 (d, 4H, J^{3}_{HH}=7.7 Hz, aryl -CH (*meta*)), 7.45 (t, 2H, J^{3}_{HH}=7.7 Hz, aryl -CH (*para*)), 7.54 (s, 2H, pyridyl -CH). ^{13}C{^{1}H} NMR (126 MHz, CD_2Cl_2, -15°C): δ(ppm) 22.8 (-CH_3, *i*-Pr), 24.2 (-CH_3, *i*-Pr), 29.9 (-CH_3, *p*-OCH_3), 58.4 (-CH_2-), 70.6 (-CF_3), 112.7, 124.2, 130.3, 139.6, 148.8, 149.2, 169.0, 173.2.

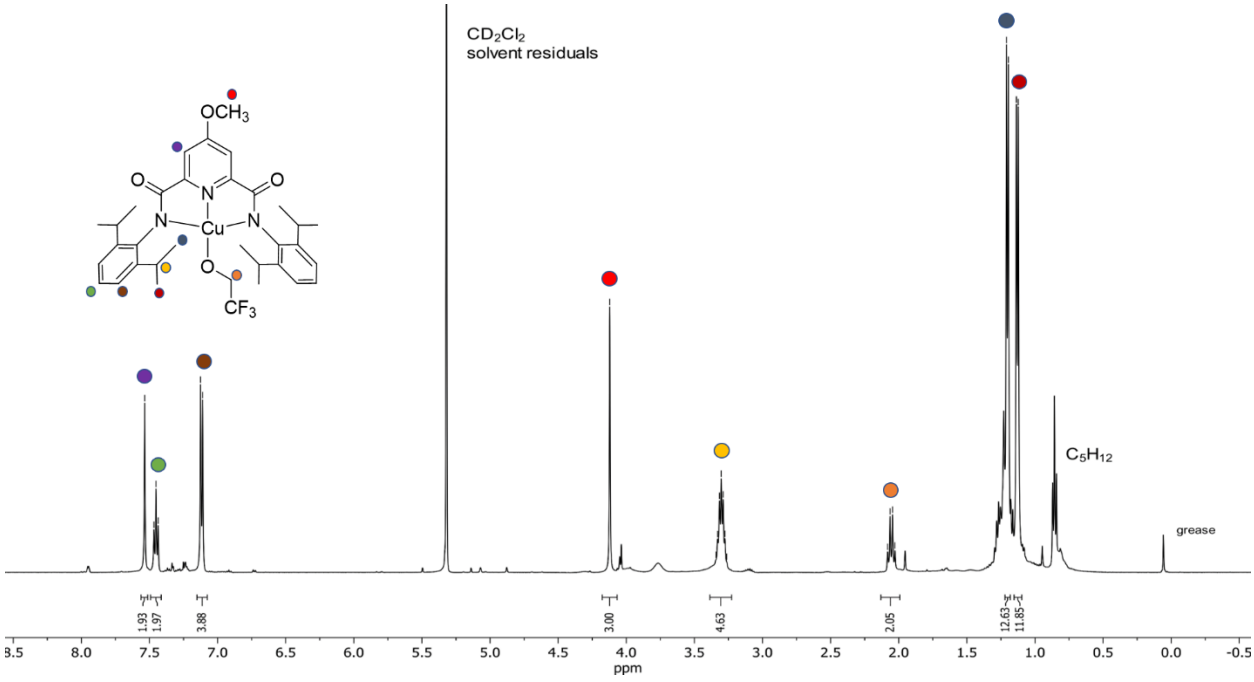

Figure S31. ^{1}H NMR spectrum of isolated crystalline $L^{OMe}CuOCH_2CF_3$ at -15 °C. Identified adventitious contaminants (pentane, silicone grease) and solvent residuals are indicated.

$^{13}C\{^{1}H\}$ NMR Spectrum of $L^{OMe}CuOCH_2CF_3$

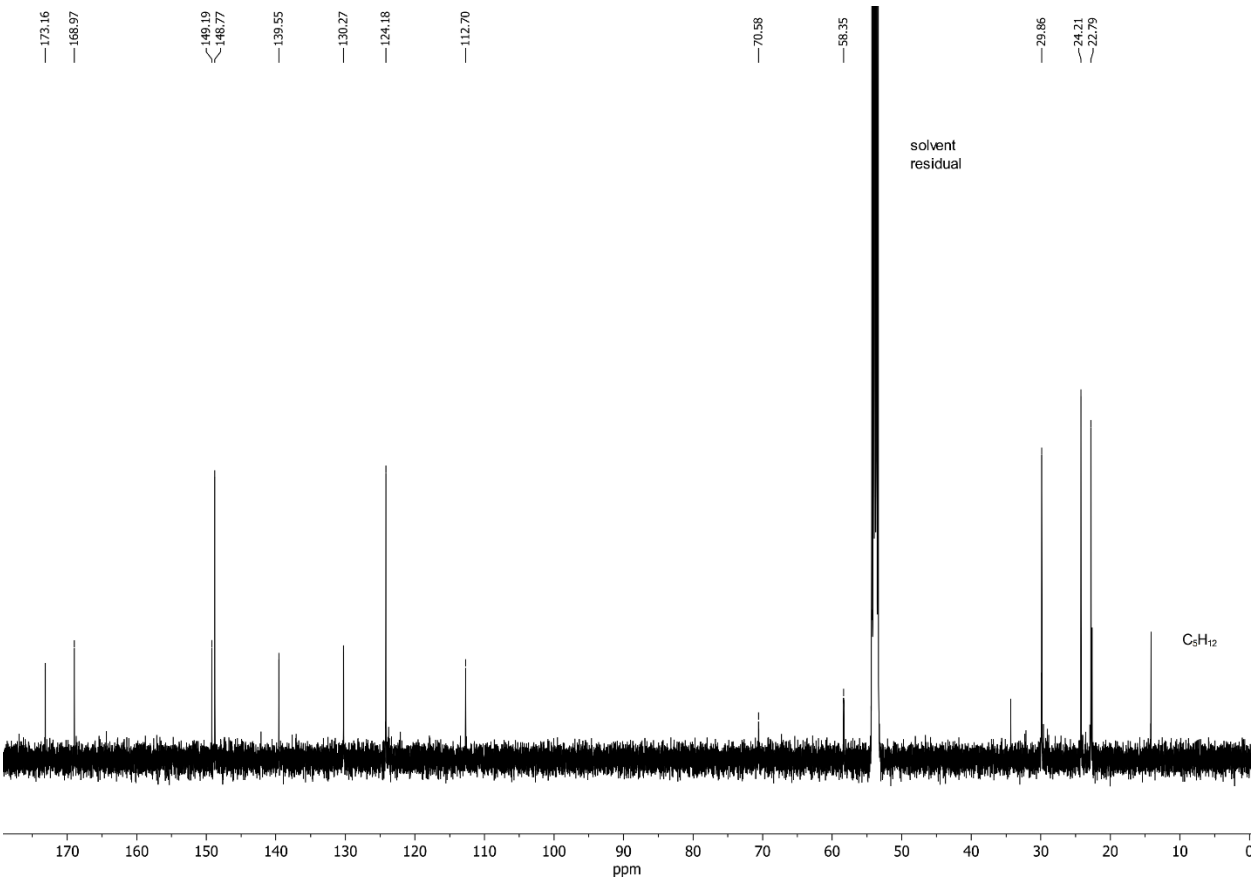

Figure S32. $^{13}C\{^{1}H\}$ NMR spectrum of isolated $L^{OMe}CuOCH_2CF_3$ at -15 °C. The isopropyl -CH signal is obscured by CD_2Cl_2 solvent residuals. Solvent residuals and adventitious solvents are indicated.

VII. SOLUTION STABILITY OF OXIDIZED Cu SPECIES

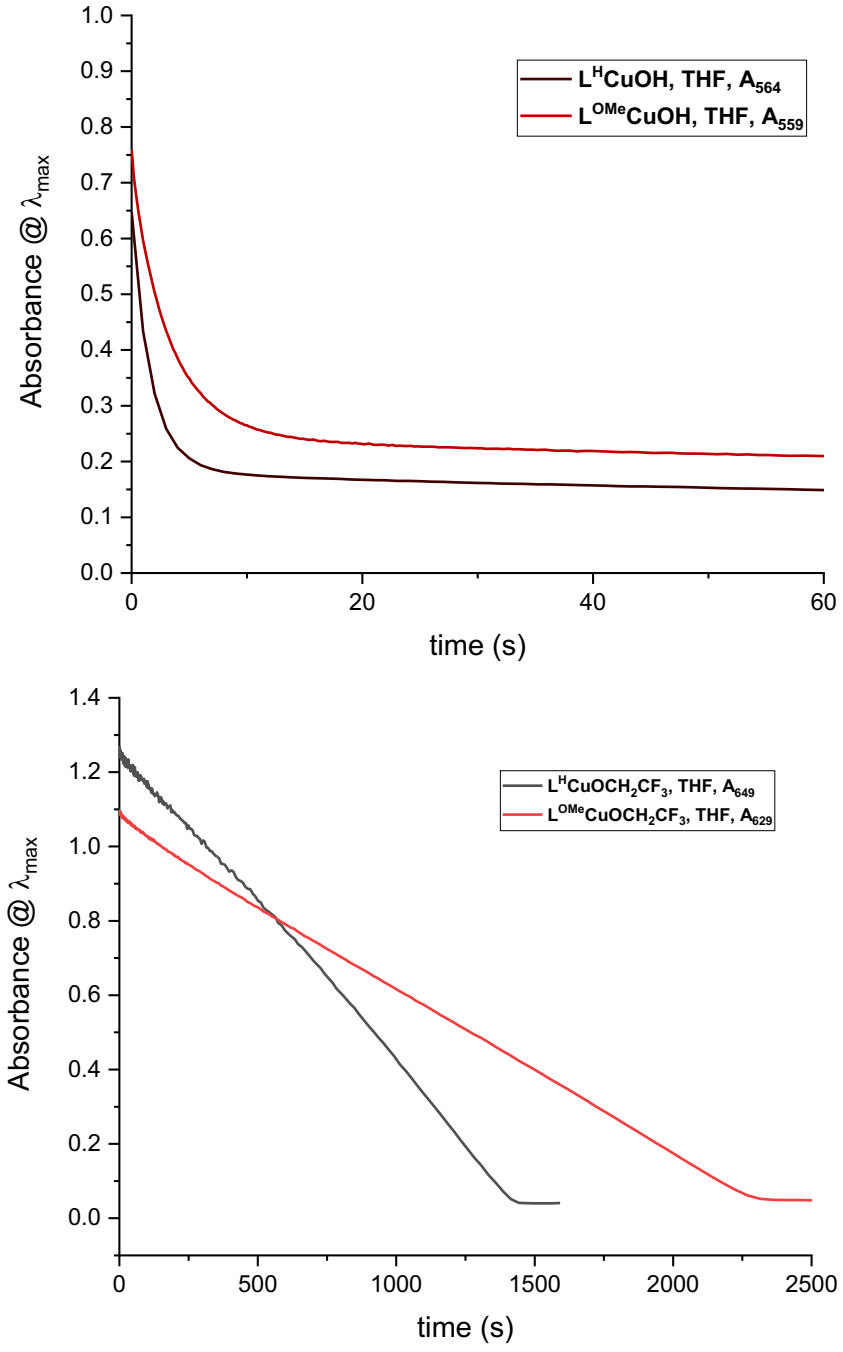

Figure S33. UV-Vis traces of the room temperature self-decay (in THF) of $[CuOH]^{2+}$ compounds (top) and $[CuOCH_2CF_3]^{2+}$ compounds (bottom). Traces are plotted with respect to the observed λ_{max} of each complex.

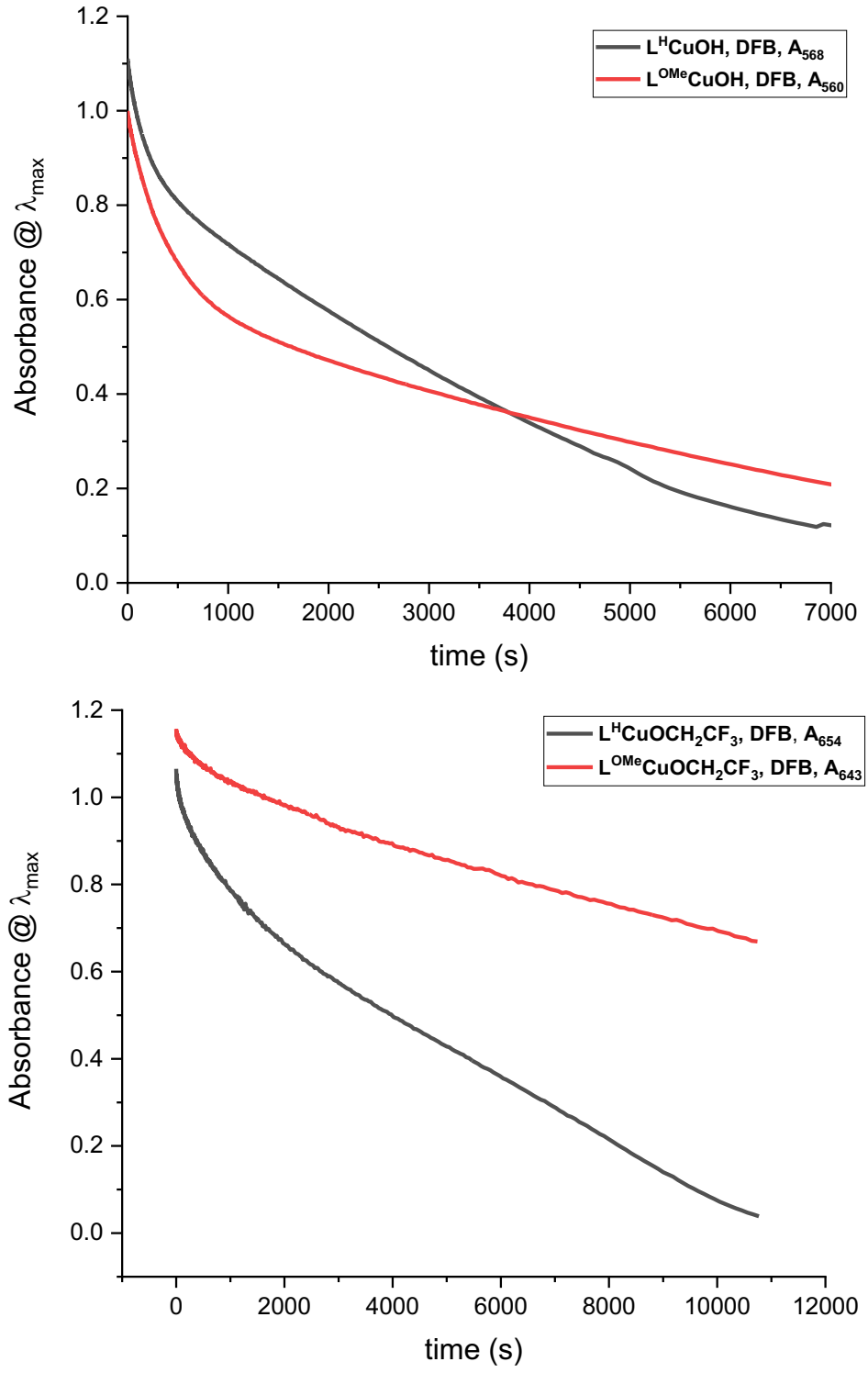

Figure S34. UV-Vis traces of the room temperature self-decay (in DFB) of $[CuOH]^{2+}$ compounds (top) and $[CuOCH_2CF_3]^{2+}$ compounds (bottom). Traces are plotted with respect to the observed λ_{max} of each complex.

Analysis of Room Temperature Self-Decay Experiments

We compared the stabilities of the four $[CuOR]^{2+}$ species by spectroscopically monitoring their room-temperature self-decays in THF and 1,2-difluorobenzene (DFB). The kinetic traces in general suggest that the decay process is complex and involves multiple mechanisms, as they display varying combinations of linear and curved (exponential) components. We therefore offer no mechanistic proposals for decay pathways and present these data in the context of elucidating comparative solution stability among the four studied complexes. Trends in the overall lifetimes of the four complexes are evident: Employing L^{OMe} and $-OCH_2CF_3$ both lead to an increase in stability, in varying amounts under different solvent conditions.

In THF, both $L^{H}CuOH$ and $L^{OMe}CuOH$ decay rapidly and mostly exponentially, with the bulk of the decay process happening over 10 s. The trifluoroethoxides $L^{H}CuOCH_2CF_3$ and $L^{OMe}CuOCH_2CF_3$, on the other hand, decay much more slowly, and, curiously, along a linear trajectory that suggests zeroth-order decay with respect to [Cu]. Under the typically utilized concentration of 0.1 mM, observed lifetimes are around 1400 s for the former and 2300 s for the latter. Overall, in THF, varying the auxiliary ligand from hydroxide to trifluoroethoxide makes a much greater impact on lifetime than does changing the supporting ligand from L to L^{OMe}.

In DFB, the range of variations is more subdued, with drastically longer lifetimes in all cases. The two hydroxide complexes decay similarly quickly overall, but along different complex curves featuring pseudo-exponential and linear regimes. $L^{H}CuOH$ decays more steadily, whereas $L^{OMe}CuOH$ decays more rapidly in the initial pseudo-exponential regime, but slows down significantly beyond 1000 s. This leads to approximately 13% $L^{OMe}CuOH$ remaining after 2 h, whereas there was no more than 4% $L^{H}CuOH$ left after the same time. Between the two trufluoroethoxides, on the other hand, there was a much more pronounced difference: While $L^{H}CuOCH_2CF_3$ decayed completely in 3 h, $L^{OMe}CuOCH_2CF_3$ had only decayed to 58%, a level

that the former compound reached in under 3000 s. All in all, in the oxidation-resistant solvent environment provided by DFB, both ligand modifications bring comparable improvements to the lifetime of the $[CuOR]^{2+}$ state, and the combination of both results in the greatest stability.

VIII. PHENOL REACTIVITY OF $[CuOR]^{2+}$ SPECIES

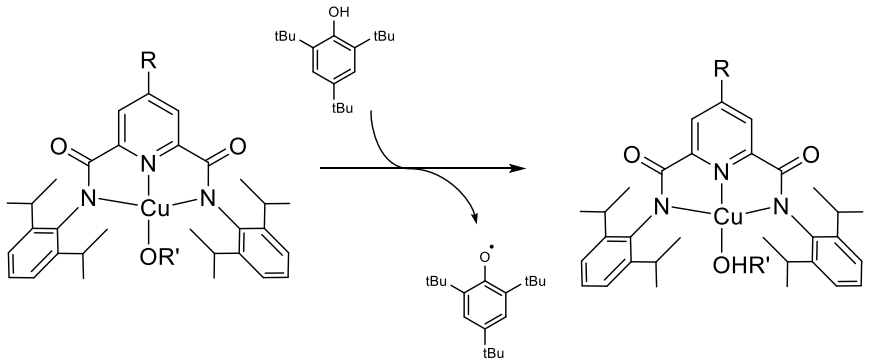

R = -H, -OCH_3
R' = -H, -OCH_2CF_3

General procedure for the reaction of $[CuOR]^{2+}$ complexes with ^{ttb}PhOH

In a glovebox, a cuvette containing DFB (1.7 mL) is outfitted with a septum and placed in a UV-Vis cell pre-cooled to -25 °C. The solution is allowed to cool for 7-15 minutes at this temperature. At this time, a solution of the corresponding Cu(II) species (0.1 mL, 2mM in DFB) is injected, and the initial spectrum taken. To this solution, a solution of oxidant ($FcBAr^F_4$ or $AcFcBAr^F_4$, 0.1 mL, 2mM) is added to generate the active $[CuOR]^{2+}$ species; once the species is observed to have fully formed, a solution of 2,4,6-tri-tert-butylphenol (^{ttb}PhOH, 0.1 mL, 2mM or 100mM) is added, causing a decay of $[CuOR]^{2+}$ signal. Decay spectra were collected and k_2 values calculated using ReactLab v1.1 with the concentrations described above. Reaction spectra, along with representative fit plots for each reaction, are shown below. Calculations for $[CuOH]^{2+}$ species were performed using 1.1 eq of ^{ttb}PhOH.

Table S1. Rate constants for $L^{Y}CuOR$ + $^{ttb}PhOH$ reaction.[a]

Trial Number	$L^{H}CuOH$ (+ 1eq $^{ttb}PhOH$)	$L^{OMe}CuOH$ (+ 1eq $^{ttb}PhOH$)	$L^{H}CuOCH_2CF_3$ (+ 50eq $^{ttb}PhOH$)	$L^{OMe}CuOCH_2CF_3$ (+ 50eq $^{ttb}PhOH$)
1	13300	9220	3.0	1.5
2	17300	13100	2.8	1.7
3	17300	13000	3.0	1.4
Average	15900	11800	3.0	1.5

[a] Individual k_2 values for the reaction of $[CuOR]^{2+}$ complexes with ttbPhOH, in units $M^{-1}s^{-1}$. Equivalents of ttbPhOH used are indicated.

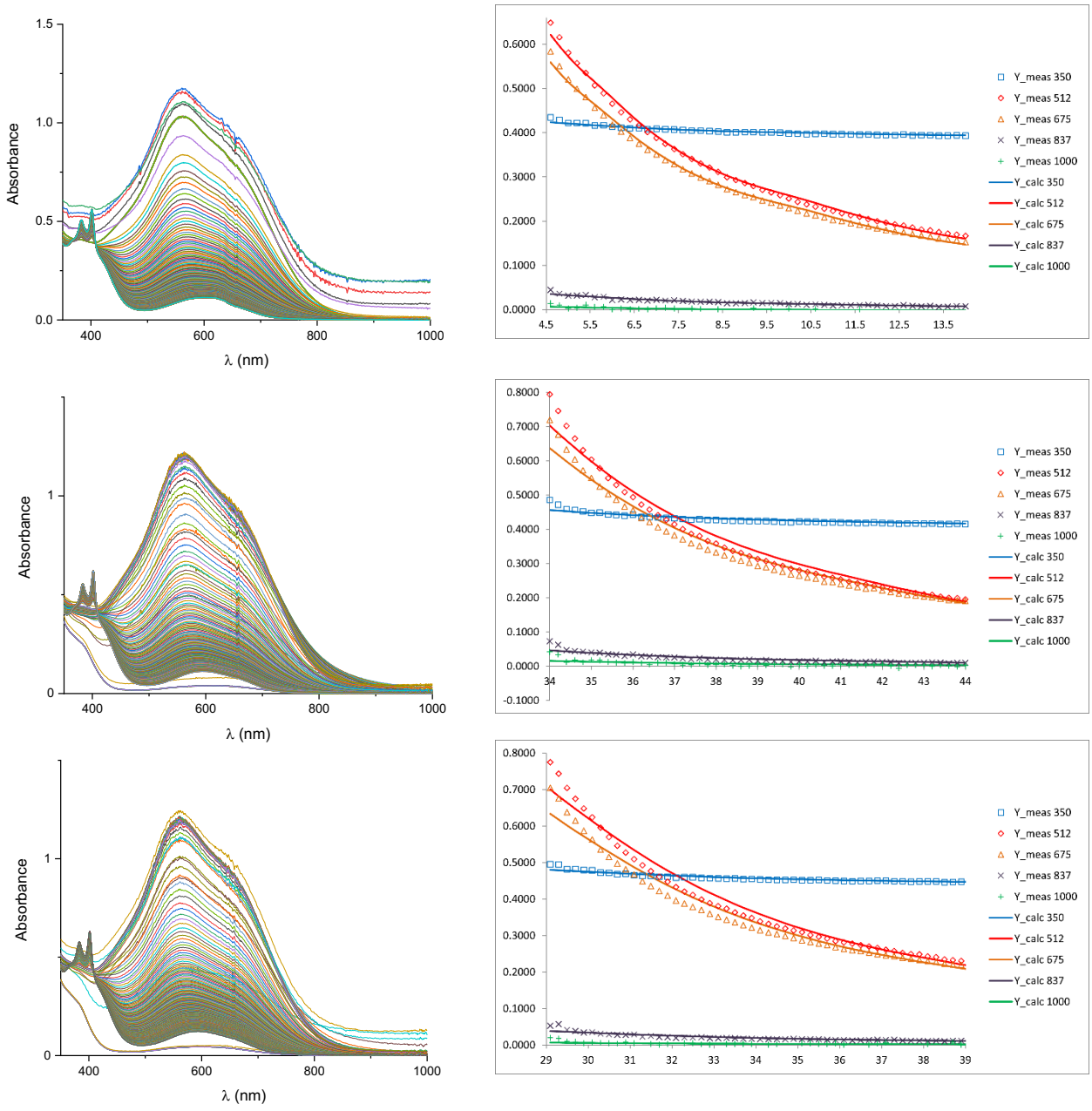

Figure S35. Triplicate UV-Vis reaction traces of $L^{H}CuOH$ + $^{ttb}PhOH$ (1 eq), DFB, -25 °C. The ensemble reaction traces are plotted on left, and the corresponding second-order model fits are shown to the right (Absorbance vs. Time (s)).

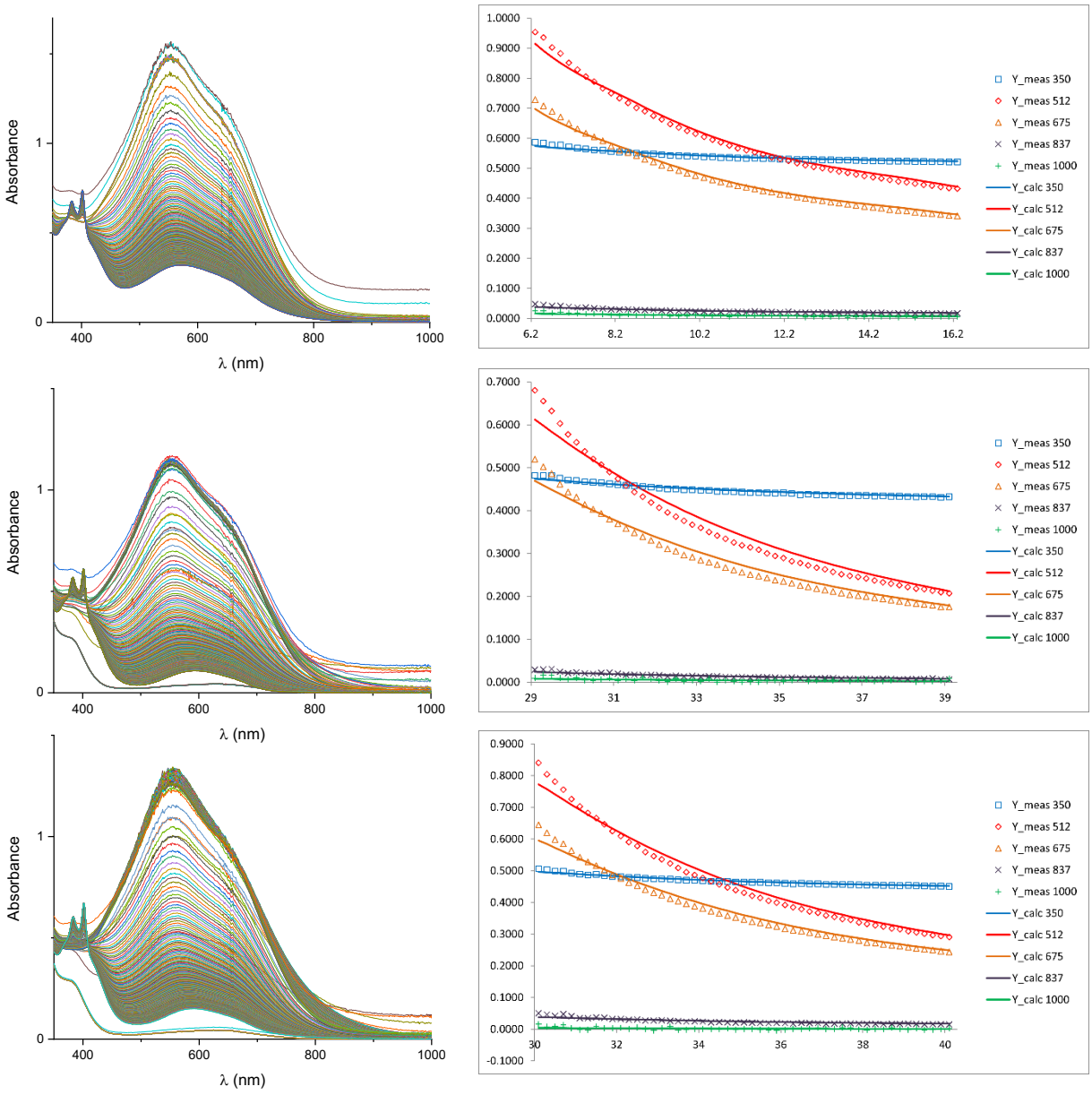

Figure S36. Triplicate UV-Vis reaction traces of $L^{OMe}CuOH$ + $^{ttb}PhOH$ (1 eq), DFB, -25 °C. The ensemble reaction traces are plotted on left, and the corresponding second-order model fits are shown to the right (Absorbance vs. Time (s)).

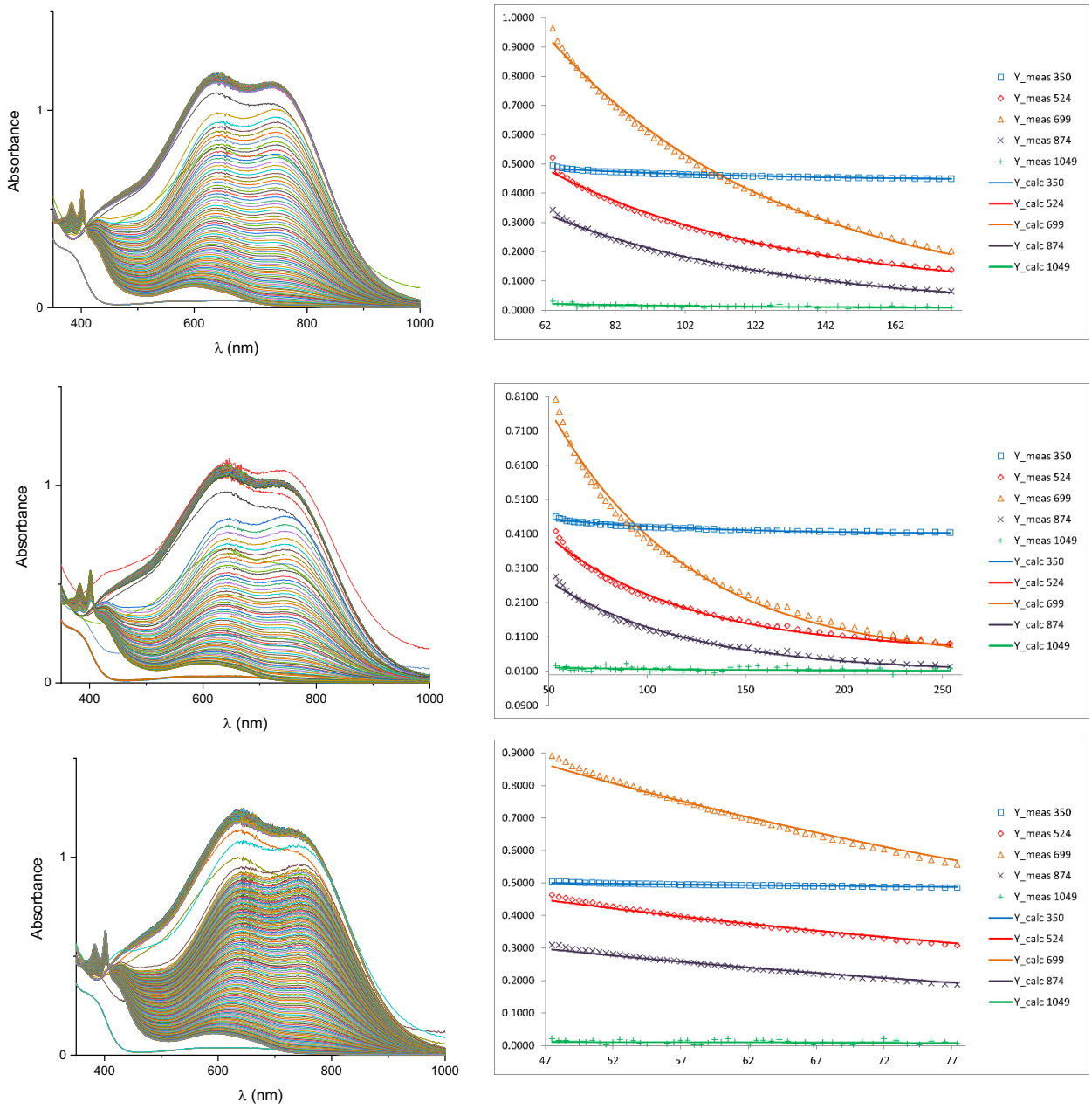

Figure S37. Triplicate UV-Vis reaction traces of $L^{H}CuOCH_2CF_3$ + $^{ttb}PhOH$ (50 eq), DFB, -25 °C. The ensemble reaction traces are plotted on left, and the corresponding second-order model fits are shown to the right (Absorbance vs. Time (s)).

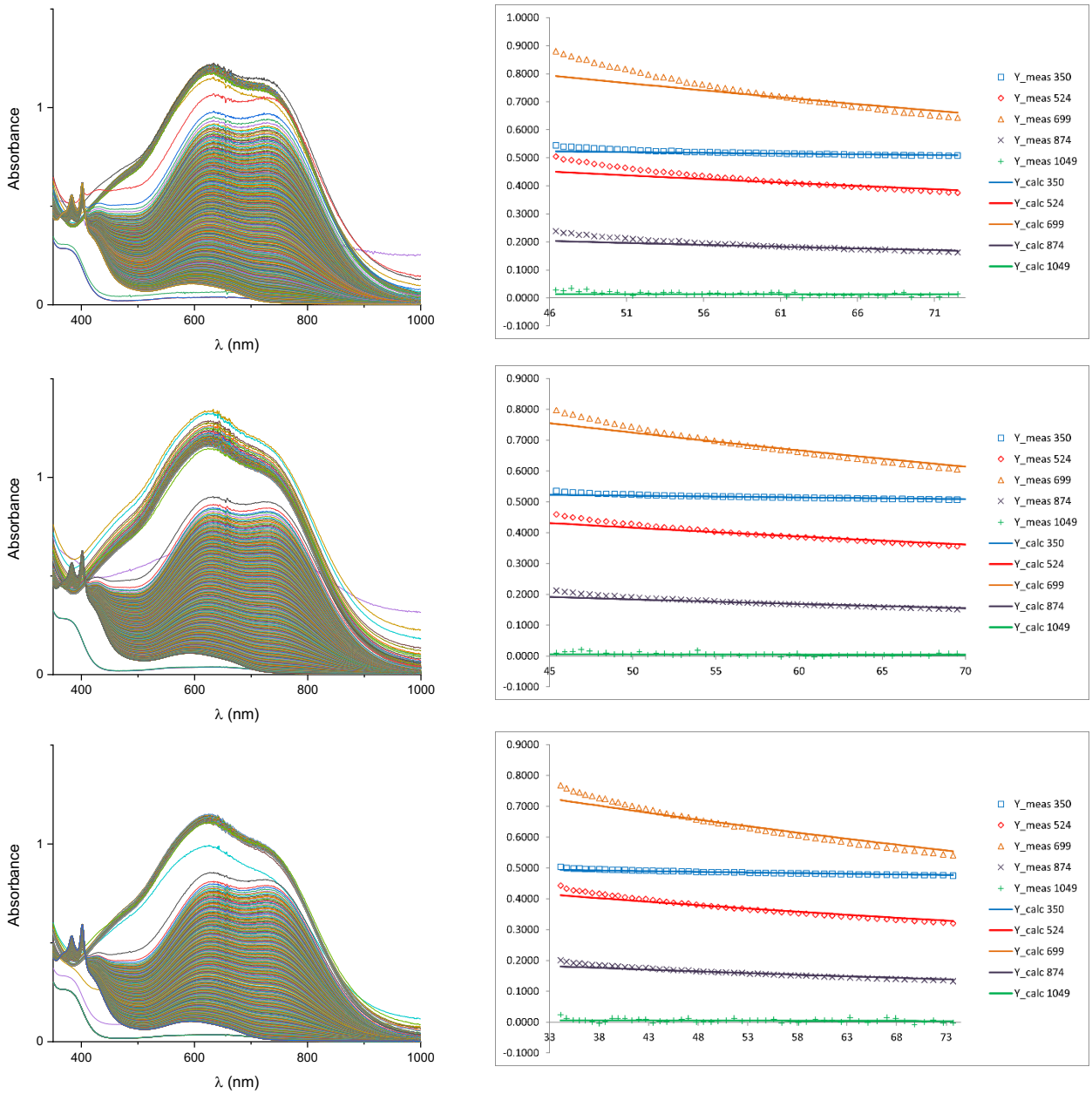

Figure S38. Triplicate UV-Vis reaction traces of $L^{OMe}CuOCH_2CF_3$ + $^{ttb}PhOH$ (50 eq), DFB, -25 °C. The ensemble reaction traces are plotted on left, and the corresponding second-order model fits are shown to the right (Absorbance vs. Time (s)).

IX. CRYSTALLIZATION AND ISOLATION OF $[CuOR]^{2+}$ SPECIES

$L^{OMe}CuOH$

$[NBu_4][L^{OMe}CuOH]$ (20 mg, 0.24 mmol) was dissolved in 1,2-DFB (0.5 mL) and cooled to -30 °C. To this solution, a cooled solution of $FcBAr^F{}_4$ (25 mg, .0.24 mmol, 1 eq) in 1,2-DFB (0.5 mL) was added, immediately producing an ink-like purple solution. This solution was layered with pentane (~18 mL) and placed at -30 °C. Dark violet-red crystals of $L^{OMe}CuOH$ surrounded by a light brown-green viscous mass (presumably $NBu_4BAr^F{}_4$ and decay products) were observed in 24h. The sample was then stored at -80 °C until data collection. Crystals also formed spontaneously in minutes when glassware containing leftover product solution (prior to addition of pentane) was left exposed to atmosphere (inert or ambient). Attempts to isolate $L^{OMe}CuOH$ from the oily residue were unsuccessful, but the latter's amorphous character permitted the use of the crystals for X-ray diffraction without undue interference.

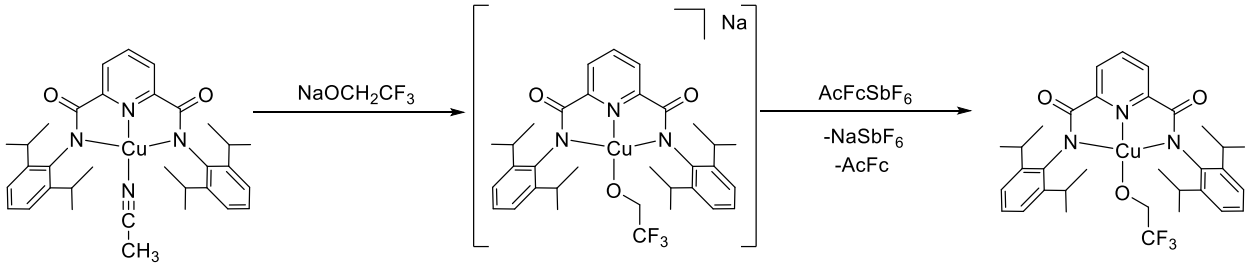

$L^{H}CuOCH_2CF_3$.

In a scintillation vial, $L^{H}CuMeCN$ (58.8 mg, 0.100 mmol) was dissolved in ca. 1.5 mL THF. A solution of $NaOCH_2CF_3$ (12.2 mg, 0.100 mmol, 1 eq.) in ca. 1.5 mL THF was added, resulting in immediate color change from reddish-brown to teal-blue. Addition of ca. 10 mL of diethyl ether resulted in partial formation of teal-blue powdery precipitation, which gave way to violet microcrystalline clumps, which over the course of ca. 1 hour consumed all colored material. After decantation, this solid was found to be poorly soluble in THF, so it was washed with THF, diethyl

ether, pentane, and dried *in vacuo*. The resulting violet powder was difficult to characterize and so was used as-is, assuming the molecular composition of $Na[L^HCuOCH_2CF_3]$ for stoichiometry purposes. We assume the color and solubility changes arose due to a transition from solution/amorphous to a packed crystalline state (crystal domains were too small for X-ray characterization).

Of the above powder, 33.5 mg (0.050 mmol) was transferred into a new scintillation vial and suspended in ca. 1.5 mL CH_2Cl_2. A suspension of $[AcFc][SbF_6]$ (23.2 mg, 0.050 mmol, 1 eq.) in ca. 1.5 mL CH_2Cl_2 was added, resulting in rapid formation of a dark blue solution with insoluble particles. After mixing for ca. 1 minute, the mixture was passed through a PTFE syringe filter along with an additional 1 mL of CH_2Cl_2. The dark blue filtrate was evaporated under reduced pressure. Approximately 5 mL of pentane was added to remove acetylferrocene, however, it turned green-blue, presumably bearing a mixture of AcFc and $L^HCuOCH_2CF_3$. A second 5 mL shot of pentane was added to the product solids and agitated, turning blue, then decanted off and set up to evaporate into heptane at -30 °C. Very small dark blue crystals began forming after 24 hours, and continued to grow as the pentane evaporated completely over several days. Despite their small size, these crystals were found to be sufficient for x-ray diffraction. Based on the appearance of the solid remaining post-extraction, the compound is only modestly soluble in pentane as the bulk remained undissolved. However, attempts to dissolve the remaining product solid in CH_2Cl_2 or mixtures of CH_2Cl_2 and pentane and precipitate by layering with pentane failed to afford any crystals. Attempts to isolate $L^HCuOCH_2CF_3$ as a pure substance were thwarted by the constant evolution of less soluble yellow-green decay species as the material was handled.

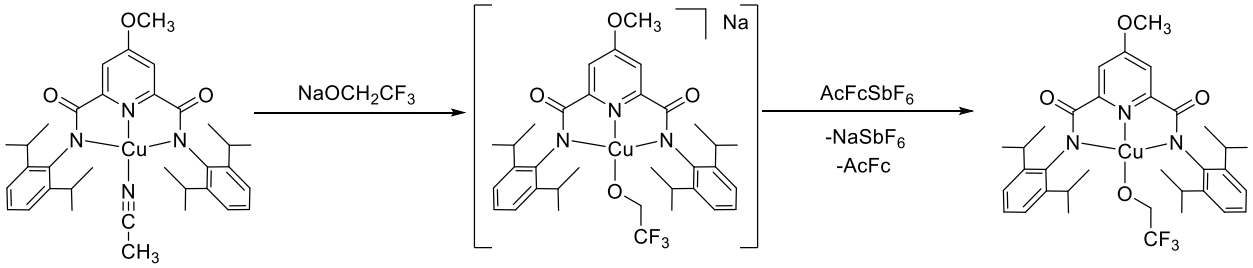

$L^{OMe}CuOCH_2CF_3$.

In a scintillation vial, L^{OMe}CuMeCN (123.6 mg, 0.200 mmol) was dissolved in ca. 1.5 mL THF. A solution of $NaOCH_2CF_3$ (24.4 mg, 0.200 mmol, 1 eq.) in ca. 1.5 mL THF was added, resulting in immediate color change from reddish-brown to teal-blue. Addition of ca. 5 mL diethyl ether and 10 mL pentane resulted in precipitation of teal-blue powder. The supernatant was decanted and the powder washed with diethyl ether and pentane, then dried *in vacuo* overnight. As with the $L^{H}CuOCH_2CF_3$ preparation, this powder was difficult to characterize and was instead used as-is, assuming a composition of Na[$L^{OMe}CuOCH_2CF_3$] for stoichiometry purposes.

Of the above powder, 64.5 mg (0.092 mmol) was transferred into a new scintillation vial and suspended in ca. 1.5 mL CH_2Cl_2. A suspension of [AcFc][SbF_6] (42.8 mg, 0.092 mmol, 1 eq) in ca. 1.5 mL CH_2Cl_2 was added, resulting in rapid formation of a dark blue solution with insoluble particles; 0.5 mL DFB was added to assist in solubilization and subsequent crystal growth (it was not found to incorporate into the crystal, however, and may not be needed). After mixing for ca. 1 minute, the mixture was passed through a PTFE syringe filter along with an additional 1 mL of CH_2Cl_2 into a scintillation vial. The dark blue filtrate was evaporated under reduced pressure to approximately 1 mL in volume, then layered with ca. 20 mL of pentane, and stored at -30 °C. After 48 hours, the entire volume appeared dark blue; the extent of crystallization was unclear but it was evident that the compound was challenging to precipitate. The top third of the solution was removed and replaced with pentane, then the mixture was again stored at -30 °C. After 24 hours,

the procedure was repeated, and after another 24 hours the mother liquor was dark green, but with solid clearly visible. After decanting ca. 90% of the liquid, replacing with pentane, mixing and repeating twice, the solid, comprised of large chunks of dark violet crystalline material with a golden semi-metallic shine, was considered "isolated" but stored under pentane at -30 °C in order to prevent loss of crystallinity. Samples of the material used for NMR, elemental analysis, and UV-visible spectroscopy were dried *in vacuo* prior to use. Individual crystals from these masses were of sufficient quality for x-ray diffraction.

Elemental analysis of the material was attempted but failed due to deviation in the amount of carbon found (Anal. calcd (%) for $C_{34}H_{41}CuF_3N_3O_4$ (MW 676.26): C 60.39, H 6.11, N 6.21; Found: 62.15, H 6.24, N 6.27). ^{1}H NMR (section VI) and UV-visible spectroscopy (**Figure S39**) indicate that the material as a bulk is composed of primarily $L^{OMe}CuOCH_2CF_3$ and small amounts of Cu(II) decay products.

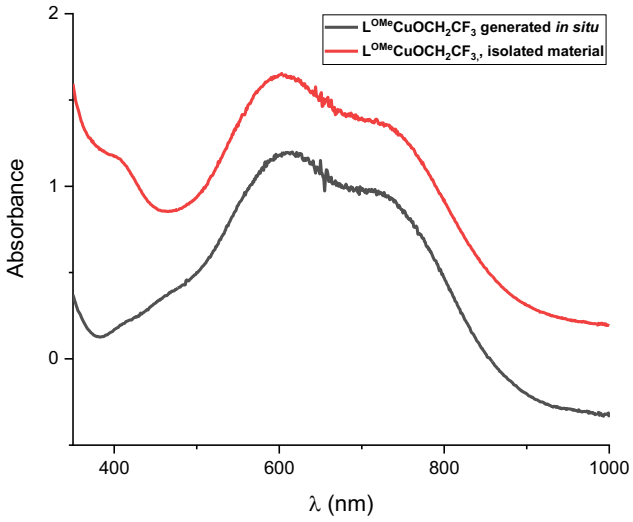

Figure S39. UV-Vis spectrum of $L^{OMe}CuOCH_2CF_3$, isolated. A spectrum of $L^{OMe}CuOCH_2CF_3$ generated *in situ* from $[NBu_4][L^{OMe}CuOCH_2CF_3]$ is shown for comparison.

X. X-RAY CRYSTALLOGRAPHY

X-ray diffraction measurements were collected with a Mo Kα or Cu Kα source on either a Bruker D8 VENTURE diffractometer equipped with a Photon II CPAD using normal parabolic mirrors as monochromators or a Bruker X8 diffractometer equipped with a Kappa Apex II CCD using a graphite monochromator. Data collection and processing was performed within the Bruker APEX3[11] software suite, using SAINT[11] for data reduction and SADABS[12] for scaling an absorption correction. Structure solutions were performed with SHELXT[13] or SHELXS[14] using OLEX 2[15] or ShelXle[16] as graphical interfaces. The structures were refined against F^2 on all data by full matrix least squares with SHELXL (see cif files for structure-specific details).[14] Non-merohedral twinning was present in the data of $L^{H}CuOCH_2CF_3$, necessitating additional steps: Domain assignment of reflections for unit cells determination was performed manually, and TWINABS[12] was used to process and scale the integrated data. The structures have been deposited to the CCDC; the accession numbers are 2053118-2053123.

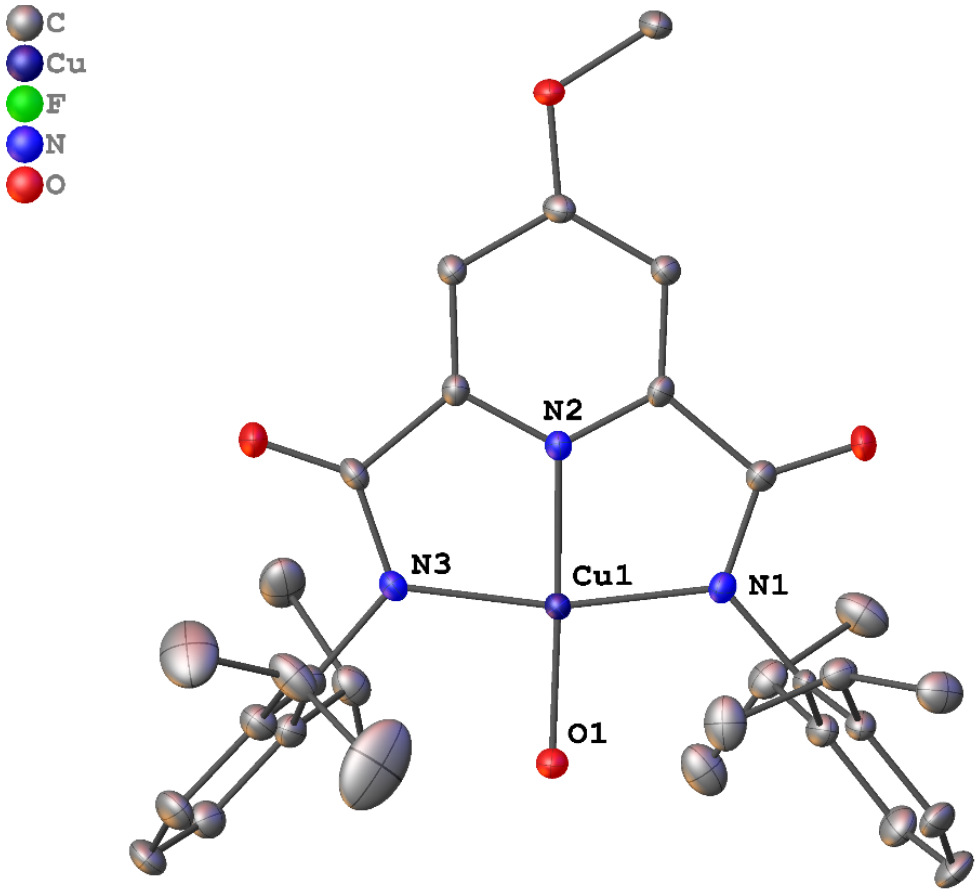

Figure S40. Thermal ellipsoid diagram of $L^{OMe}CuOH \cdot 2DFB$, showing all nonhydrogen atoms at 50% probability level. Two 1,2-difluorobenzene molecules have been omitted for clarity.

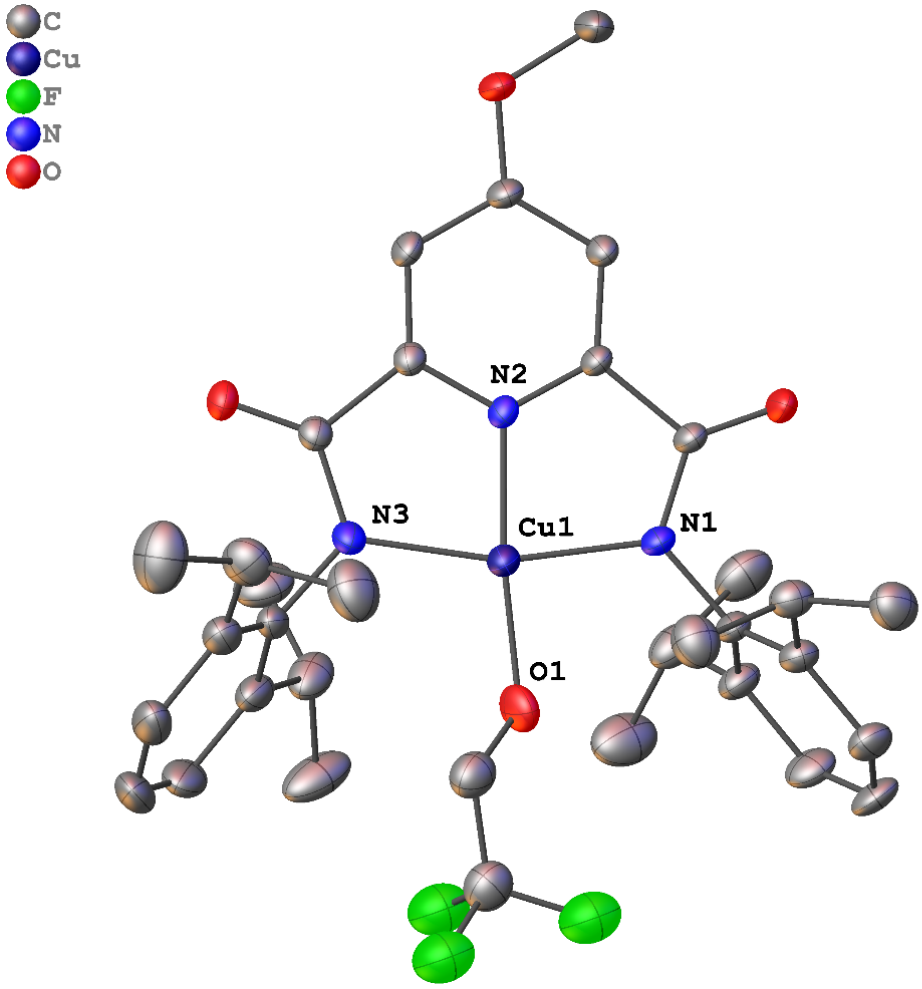

Figure S41. Thermal ellipsoid diagram of $L^{OMe}CuOCH_2CF_3$, showing all nonhydrogen atoms at 50% probability level. Only one of two disordered orientations of the -OCH_2CF_3 group is shown.

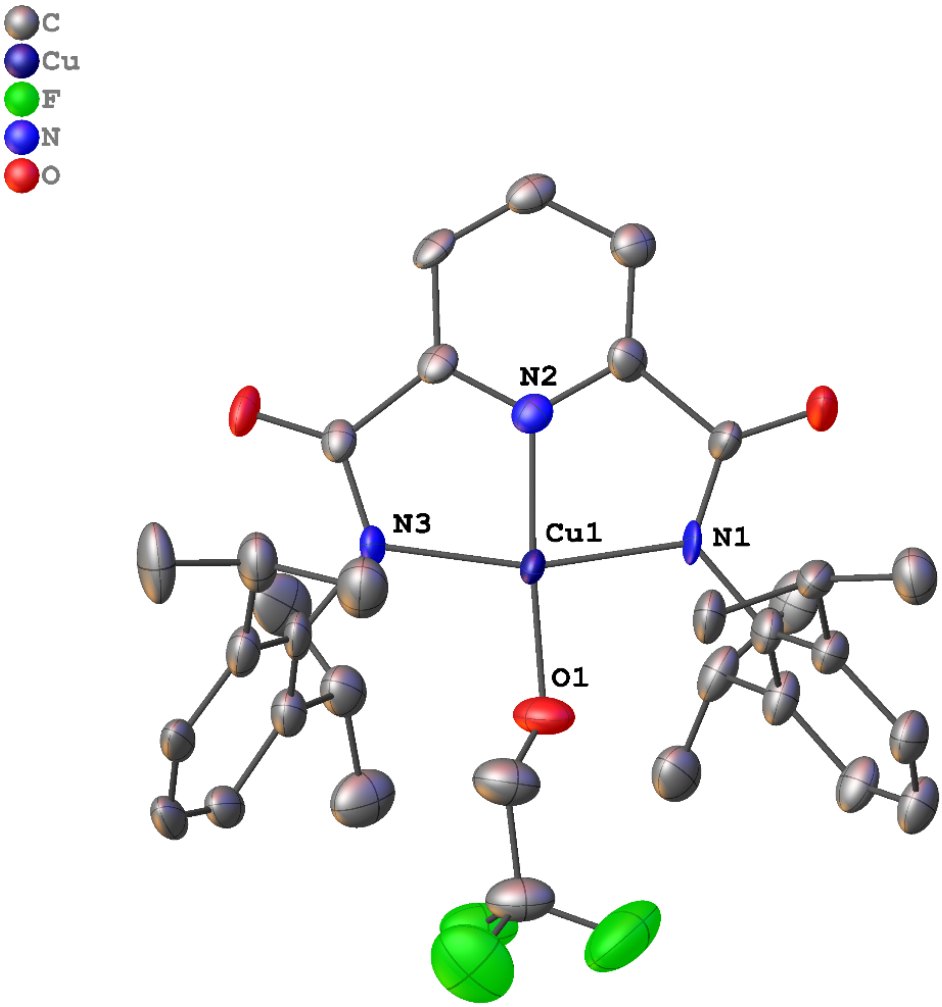

Figure S42. Thermal ellipsoid diagram of $L^{H}CuOCH_2CF_3$, showing all nonhydrogen atoms at 50% probability level.

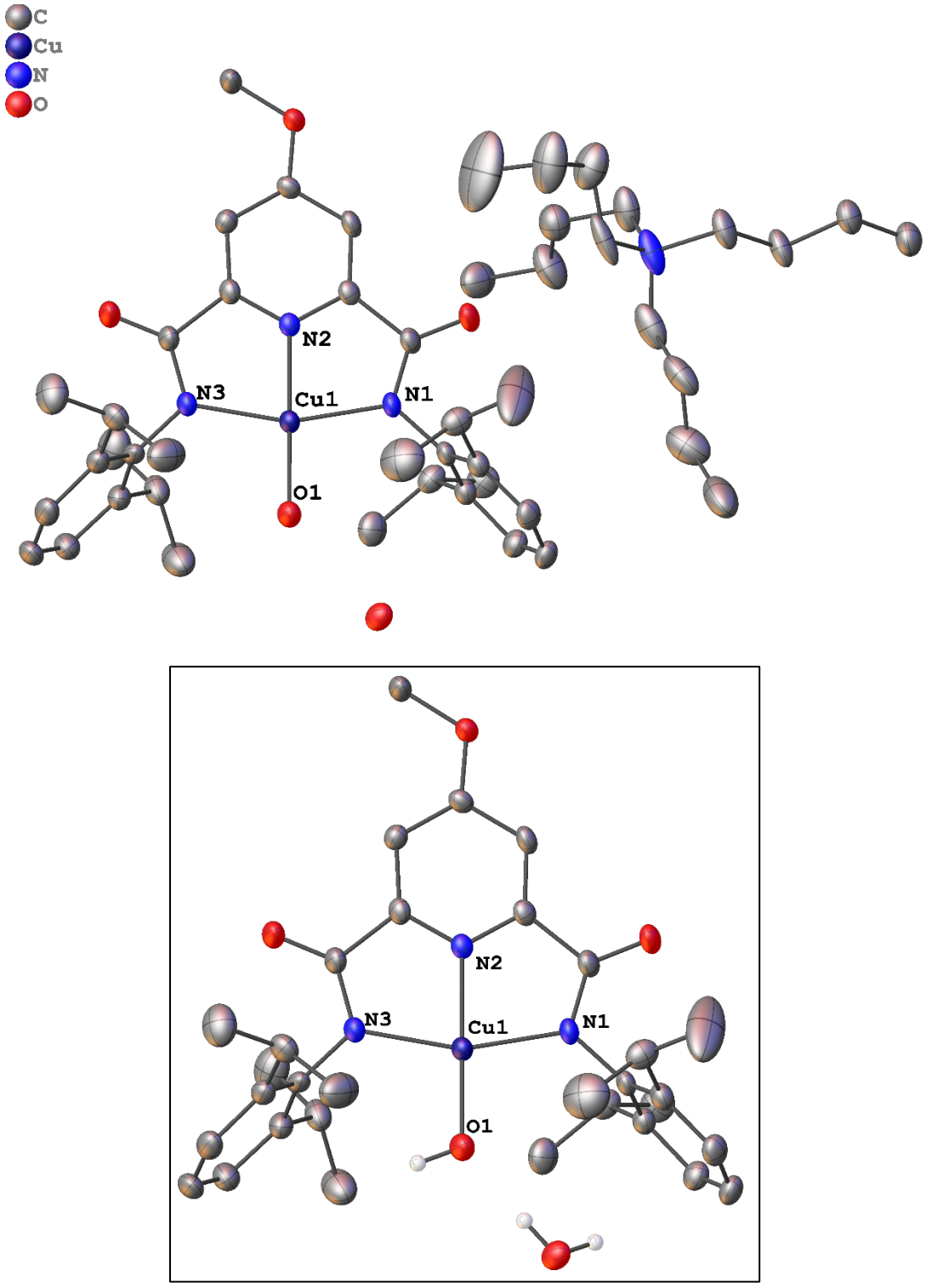

Figure S43. Top: Thermal ellipsoid diagram of $[NBu_4][L^{OMe}CuOH]\cdot H_2O\cdot Et_2O$, showing all nonhydrogen atoms at 50% probability level. One diethyl ether molecule, as well as disorder in NBu_4^+ and one of the isopropyl groups of L^{OMe}, are not shown for clarity. Bottom: Hydrogen atoms of -OH and H_2O displayed to show hydrogen bonding.

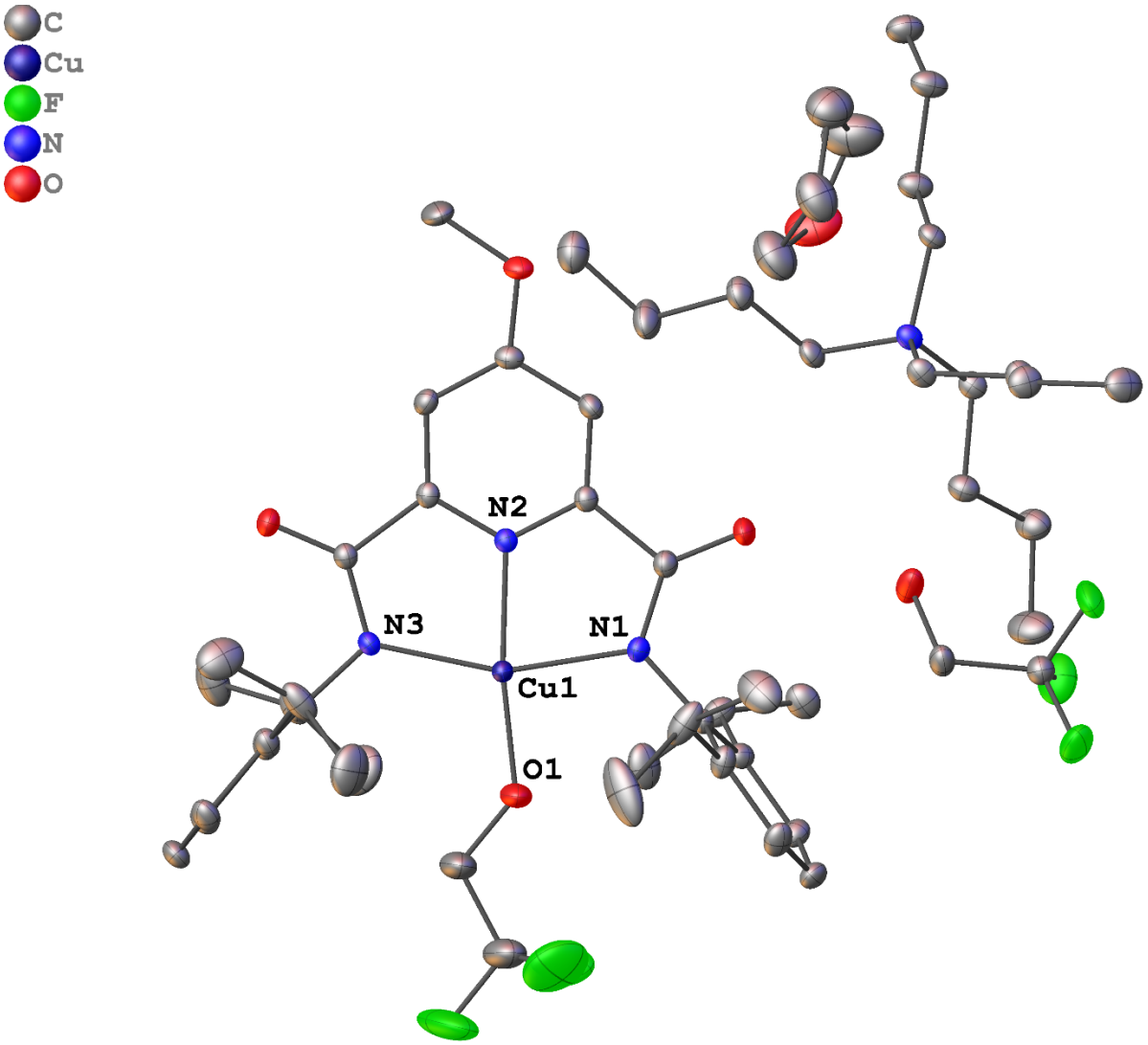

Figure S44. Thermal ellipsoid diagram of $[NBu_4]L^{OMe}CuOCH_2CF_3]\cdot CF_3CH_2OH\cdot THF$, showing all nonhydrogen atoms at 50% probability level. Only one of two disordered orientations of the -OCH_2CF_3 group is shown.

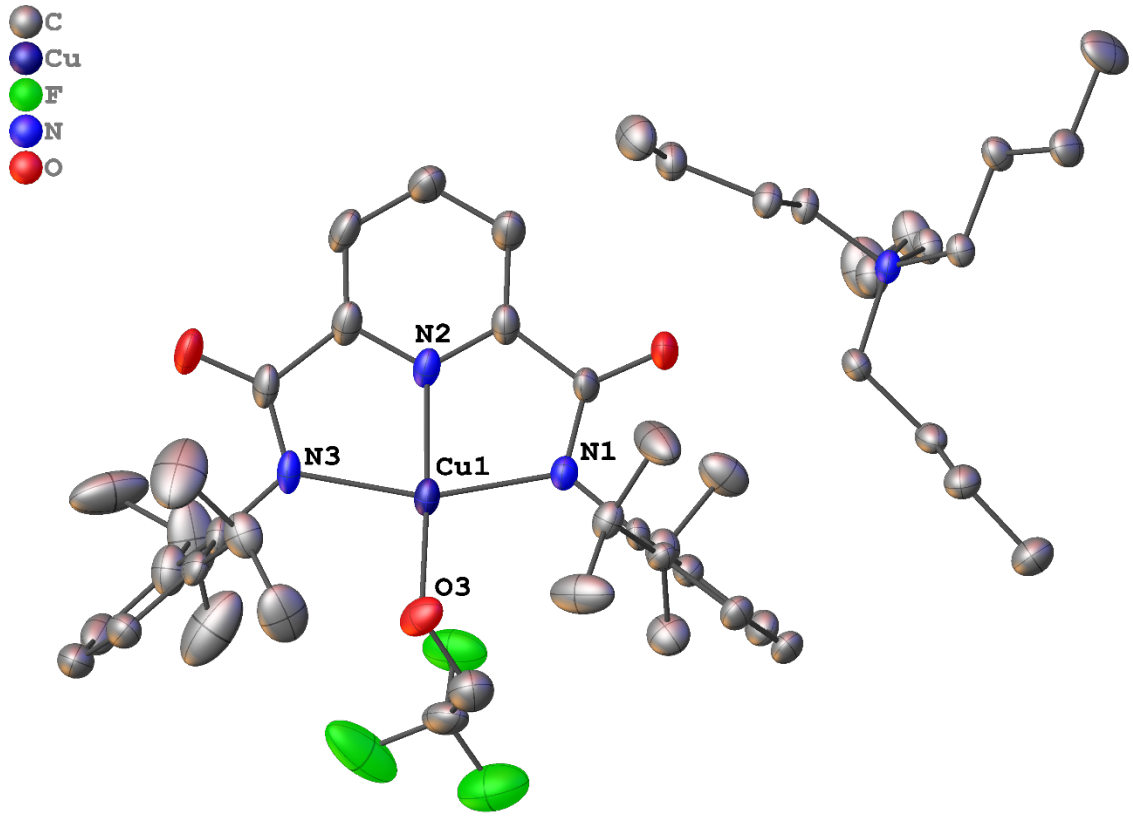

Figure S45. Thermal ellipsoid diagram of $[NBu_4]LCuOCH_2CF_3]\cdot C_5H_{12}$, showing all nonhydrogen atoms at 50% probability level. One pentane molecule has been omitted for clarity

XI. RESONANCE RAMAN SPECTROSCOPY OF $L^{Y}CuOR$

General Comments:

Resonance Raman spectra were obtained by collecting the collimated Raman scattering using a Plano convex lenses (f = 10cm, placed at an appropriate distance) through a long-pass edge filter (Semrock). The spectra were collected by an Andor ShamrockSR-500i monochromator with a Newton 920 thermo-electrically cooled CCD detector (DU920-BU) interfaced with Solis S software. The detector was cooled to -90 °C before collection. The spectra were obtained on frozen samples at 77 K using a 135° backscattering geometry. Excitation at 561nm was provided by a Cobolt Jive 150 mW laser. Raman shifts were externally referenced to indene and internally referenced to solvent (THF). Each spectrum was an accumulation of 450 spectra with 4s acquisition times, resulting in 30 min collections. Spectra were baseline corrected using a multi-point correction process using SpectraGryph.[17]

General preparation of $L^{Y}CuOR$ for Raman spectroscopy

In a glovebox, a quartz EPR tube was charged with a solution of $L^{Y}CuOR$ (Y = -H, -OMe; R = -H, $-OCH_2CF_3$, THF) and a small magnetic spin bar, sealed with a rubber septum, brought out, and cooled to -78°C (acetone/dry ice). At this time, a syringe containing 1 equivalent of oxidant ($FcBAr^{F}_4$ or $AcFcBAr^{F}_4$ in THF) was slowly injected into the cooled tube (to layer) and allowed to equilibrate to temperature; an external magnetic rod was used to manipulate the spin bar in order to mix the solution and subsequently suspend it above the liquid. The sample was then quickly removed from the cooling bath, wiped briefly to remove acetone from the outer surface, and frozen rapidly in liquid nitrogen. After the sample was adequately frozen, the septum and spin bar were removed; samples were stored at 77 K until data acquisition.

Sample preparation rR spectrum of $L^{OMe}CuOH$

The sample was prepared and spectrum acquired as described in the General Procedure (above) using 0.2 mL of $[NBu_4][L^{OMe}CuOH]$ (10mM, THF) and $FcBAr^F{}_4$ (0.25 mL, 8 mM in THF, prepared in glovebox) (Figure S46).

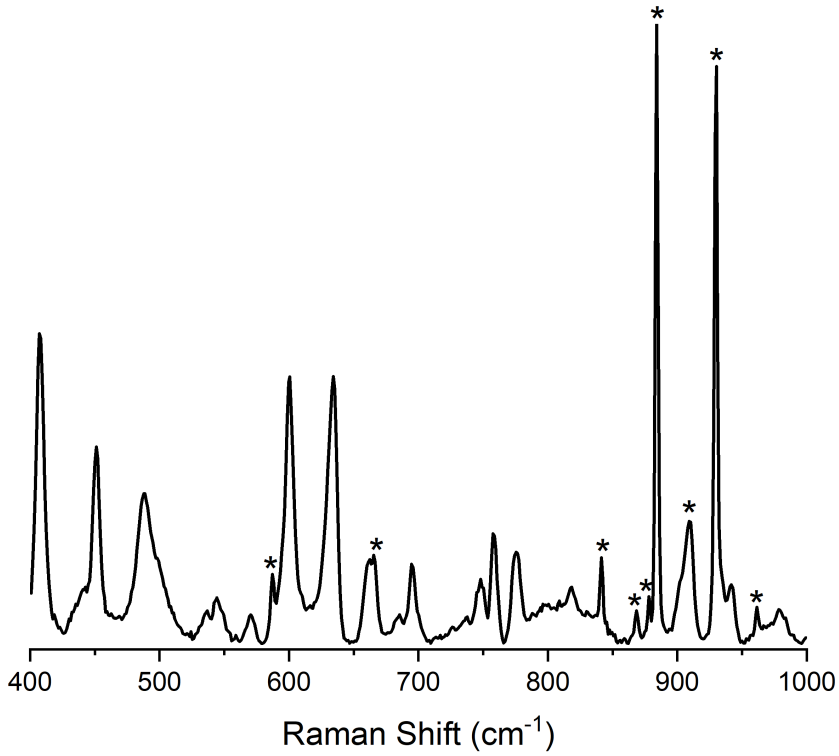

Figure S46. Resonance-enhanced Raman spectrum of $L^{OMe}CuOH$ (4.4 mM in THF)**.** $\nu_{Cu\text{-}O}$ is assigned at 634 cm^{-1} (indicated) in accordance with homologous reported systems.[17] Asterisks indicate solvent peaks.

Sample preparation rR Spectrum of $L^YCuOCH_2CF_3$ (Y = -H, -OMe)

The sample was prepared and spectrum acquired as described in the General Procedure (above) using 0.25 mL of $[NBu_4][L^YCuOCH_2CF_3]$ (8 mM, THF) and 0.25 mL of oxidant solution (8 mM, THF). $FcBAr^F{}_4$ was used for Y = -OMe (Figure S47); $AcFcBAr^F{}_4$ was used for Y = -H (Figure S48).

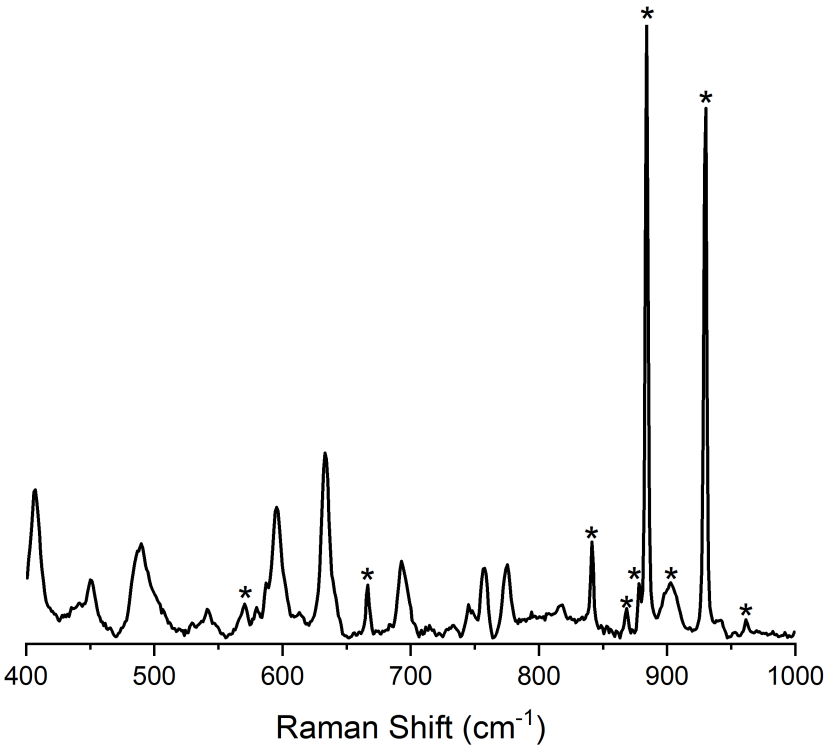

Figure S47. Resonance-enhanced Raman spectrum of $\mathbf{L}^{OMe}CuOCH_2CF_3$ (4. mM in THF)**.** $\nu_{Cu\text{-}O}$ is assigned at 634 cm^{-1} (indicated) in accordance with homologous reported systems.[18] Asterisks indicate solvent peaks.

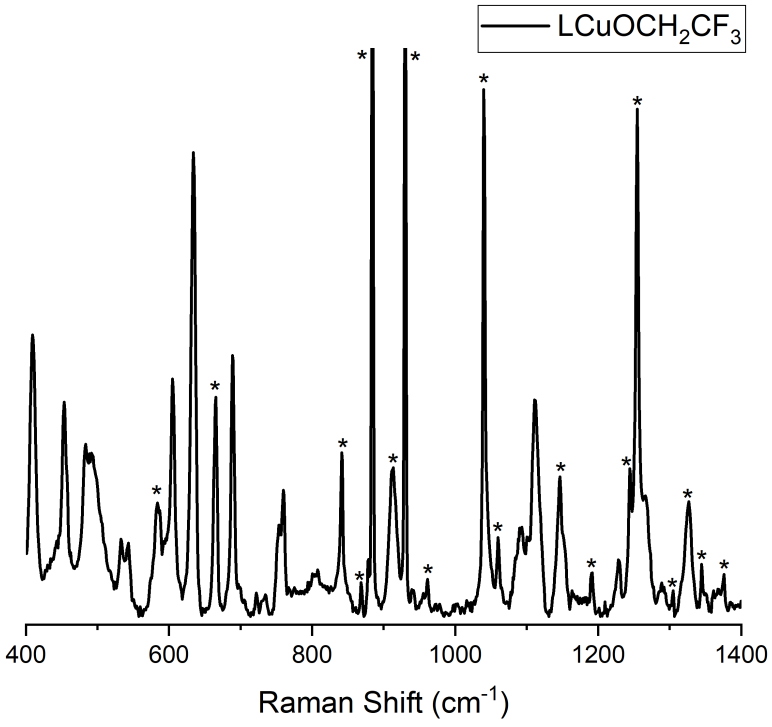

Figure S48. Frozen solution resonance Raman spectrum of 4 mM $L^{H}CuOCH_2CF_3$ in THF at 77 K

using 561 nm excitation. Asterisks indicate solvent peaks.

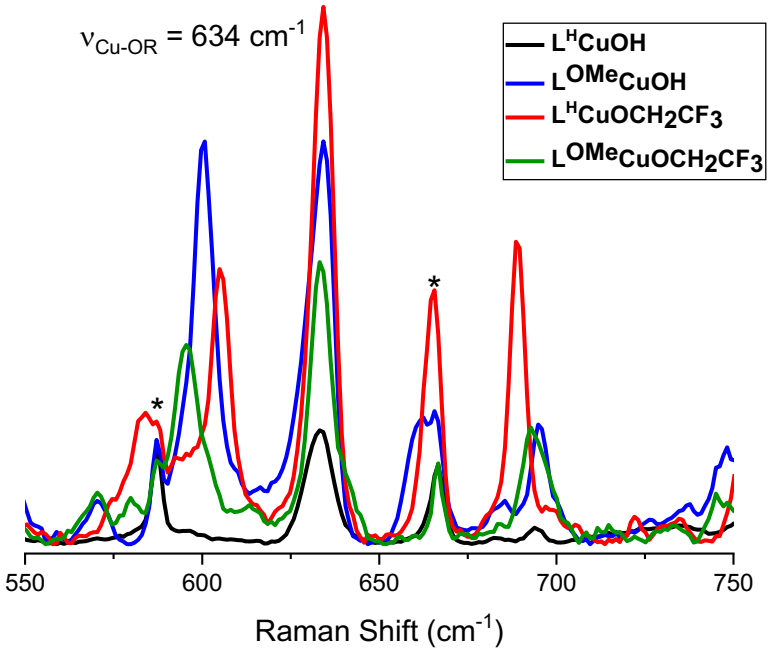

Figure S49. Overlay of $[CuOR]^{2+}$ resonance Raman spectra between 550-750 cm^{-1}. Signals attributed to ν_{Cu-OR} for each complex (located at 634 cm^{-1}) are indicated. While signal clusters located around 600 cm^{-1} and 690cm^{-1} appear to arise from the complexes, we have not assigned these peaks. However, we note the resemblance of these spectra to those of $TpCuOCH_2CF_3$ (Tp = hydro-tris(pyrazolyl)borate).[19] Asterisks indicate solvent peaks.

XII. DENSITY FUNCTIONAL THEORY

Computational Details

Gas phase geometry optimizations and harmonic vibrational frequencies were performed for the singlet ground state using the mPW1PW91 functional as implemented in Gaussian 16.[20,21] The SDD basis set and pseudopotential were used for Cu while the remaining atoms were treated with the 6-311+G(d,p) basis set.[22-24] Single point energy calculations were performed for the triplet state on the singlet optimized geometry. The Raman spectra were computed using the precomputed vibrational scaling factor of 0.957, as recommended for mPW1PW91/6-311+G(d,p).[25] Note that we use a mixed basis set and the scaling factor for mPW1PW91/SDD is 0.950; however, we have chosen the scaling factor for the basis set used for all atoms with the exception of Cu. Time dependent DFT (TDDFT) calculations were also performed using the B98 functional with the same basis set.[26,27] Transition energies were computed for the first 36 singlet states. These transitions were fit to standard Gaussian curves to determine the calculated spectra using a spectral broadening factor of 0.333 eV. We also plot the UV-vis spectra with a narrower broadening of 0.1 eV to show underlying differences between the studied complexes that are hidden using the standard broadening.

Summary of Calculated Properties

Table S2. Bond distances (Å) obtained by DFT (mPW1PW91) for $[CuOR]^{2+}$ ("Cu(III)") species. Averaged values presented for $Cu\text{-}N_1$ and $Cu\text{-}N_3$ bonds.

Bond	L, OH	L^{OMe}, OH	L, OCH_2CF_3	L^{OMe}, OCH_2CF_3
$Cu\text{-}N_2$	1.853	1.845	1.875	1.866
$Cu\text{-}N_{1,3}$	1.915	1.916	1.960	1.960
$Cu\text{-}O_1$	1.783	1.783	1.818	1.817

Table S3. The λ_{max} and oscillator strengths (f) as computed by TD-DFT (B98) for $[CuOR]^{2+}$ ("Cu(III)") species.

	L, OH	**L^{OMe}, OH**	**L, OCH_2CF_3**	**L^{OMe}, OCH_2CF_3**
λ_{max} (nm)	546.1	537.1	578.7	573.6
f	0.3194	0.3197	0.3222	0.3194

Table S4. Calculated (mPW1PW91) orbital energies for $[CuOR]^{2+}$ ("Cu(III)") species in eV.

	L, OH	**L^{OMe}, OH**	**L, OCH_2CF_3**	**L^{OMe}, OCH_2CF_3**
HOMO	-6.6412	-6.5770	-6.6388	-6.5800
LUMO	-3.7386	-3.6262	-4.0730	-3.9701
HOMO-LUMO gap	2.90	2.95	2.57	2.61

Table S5. Calculated (mPW1PW91) energy differences between the S=0 and S=1 states for $[CuOR]^{2+}$ ("Cu(III)") species in kcal/mol. Attempts to converge the broken symmetry singlet solution converged to the closed shell case for all four complexes.

	Singlet-Triplet Splitting (kcal/mol)
$L^{H}CuH$	32.25
$L^{OMe}CuH$	33.43
$L^{H}CuOCH_2CF_3$	20.59
$L^{OMe}CuOCH_2CF_3$	21.68

Table S6. CM5 atomic charges calculated at the mPW1PW91/6-311+G(d,p)/SDD level of theory.

	L, OH	**L^{OMe}, OH**	**L, OCH_2CF_3**	**L^{OMe}, OCH_2CF_3**
Cu	0.908	0.910	0.866	0.870
O	-0.614	-0.618	-0.410	-0.413
N1,3 (avg.)	-0.420	-0.419	-0.412	-0.411
N2	-0.377	-0.394	-0.368	-0.385

UV-visible Spectra

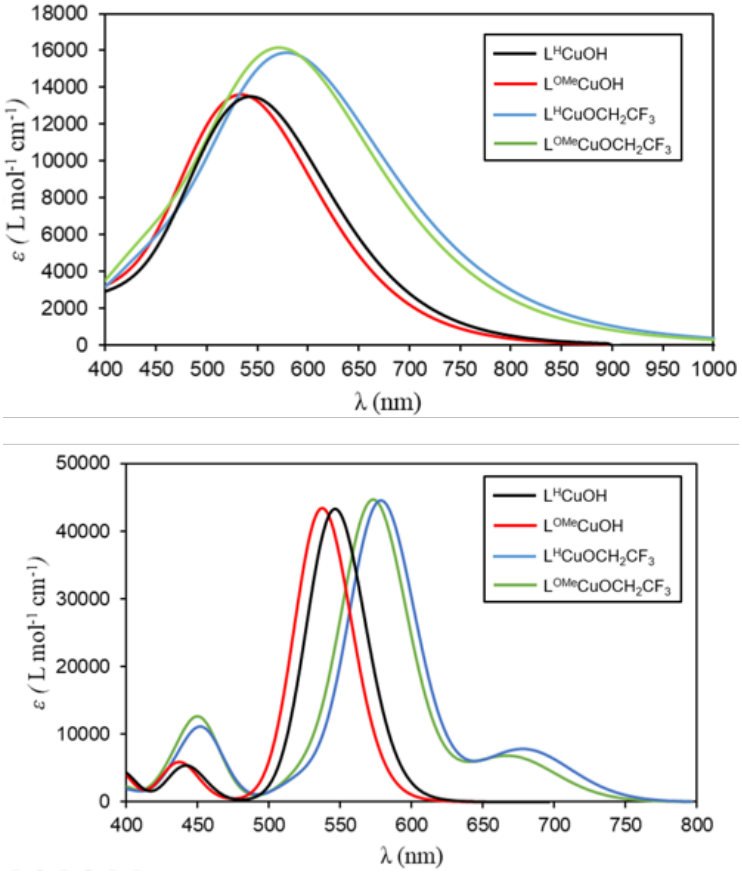

Figure S50. UV-Vis spectra computed at the B98/6-311+G(d,p)/SDD level of theory with a spectra broadening value of 0.333 eV (top) and 0.1 eV (bottom).

Table S7. Detailed description of the four lowest excited states for the L^{H}CuOH structure computed at the TD-B98/6-311+G(d,p)/SDD level of theory.

Excited State	Excitation Energy (nm)	Oscillator Strength	Transition Description	Coefficient
1	599.24	0.0008	HOMO-7 to LUMO	0.20793
			HOMO-5 to LUMO	-0.18224
			HOMO-4 to LUMO	0.53601
			HOMO-1 to LUMO	0.34719
2	588.23	0.002	HOMO-7 to LUMO	0.14969
			HOMO-5 to LUMO	-0.26616
			HOMO-4 to LUMO	-0.43599
			HOMO-1 to LUMO	0.44277
3	564.37	0.0013	HOMO-7 to LUMO	-0.27801
			HOMO-5 to LUMO	0.44035
			HOMO-2 to LUMO	0.20052
			HOMO-1 to LUMO	0.42545
4	546.09	0.3194	HOMO to LUMO	0.69613

Table S8. Detailed description of the four lowest excited states for the L^{OMe}CuOH structure computed at the TD-B98/6-311+G(d,p)/SDD level of theory.

Excited State	Excitation Energy (nm)	Oscillator Strength	Transition Description	Coefficient
1	587.8	0.0011	HOMO-7 to LUMO	0.24409
			HOMO-5 to LUMO	-0.19029
			HOMO-4 to LUMO	0.54076
			HOMO-1 to LUMO	-0.28872
2	580.8	0.0012	HOMO-7 to LUMO	-0.24126
			HOMO-5 to LUMO	0.35314
			HOMO-4 to LUMO	0.40676
			HOMO-2 to LUMO	-0.13919
			HOMO-1 to LUMO	0.33330
3	554.8	0.0029	HOMO-7 to LUMO	0.23633
			HOMO-5 to LUMO	-0.33029
			HOMO-2 to LUMO	0.15687
			HOMO-1 to LUMO	0.55030
4	537.1	0.3197	HOMO to LUMO	0.69438

Table S9. Detailed description of the four lowest excited states for the $L^{H}CuOCH_2CF_3$ structure computed at the TD-B98/6-311+G(d,p)/SDD level of theory.

Excited State	Excitation Energy (nm)	Oscillator Strength	Transition Description	Coefficient
1	679.3	0.0555	HOM0-4 to LUMO	0.55587
			HOMO-3 to LUMO	0.11181
			HOMO to LUMO	-0.38937
2	678.0	0.0012	HOMO-7 to LUMO	0.20995
			HOMO-5 to LUMO	0.44772
			HOMO-3 to LUMO	0.20929
			HOMO-2 to LUMO	-0.12367
			HOMO-1 to LUMO	0.42423
3	627.0	0.0049	HOMO-7 to LUMO	-0.13735
			HOMO-5 to LUMO	-0.3311
			HOMO-3 to LUMO	-0.18246
			HOMO-2 to LUMO	0.11929
			HOMO-1 to LUMO	0.56233
4	578.7	0.3222	HOMO-4 to LUMO	0.36126
			HOMO-3 to LUMO	0.11697
			HOMO to LUMO	0.56716

Table S10. Detailed description of the four lowest excited states for the $L^{OMe}CuOCH_2CF_3$ structure computed at the TD-B98/6-311+G(d,p)/SDD level of theory.

Excited State	Excitation Energy (nm)	Oscillator Strength	Transition Description	Coefficient
1	674.9	0.0199	HOMO-7 to LUMO	0.13140
			HOMO-6 to LUMO	-0.24166
			HOMO-5 to LUMO	0.36052
			HOMO-4 to LUMO	-0.34913
			HOMO-3 to LUMO	0.12937
			HOMO-1 to LUMO	0.29326
			HOMO to LUMO	0.21375
2	665.4	0.0299	HOMO-5 to LUMO	0.25672
			HOMO-4 to LUMO	0.45845
			HOMO-3 to LUMO	0.20862
			HOMO-2 to LUMO	-0.10959
			HOMO-1 to LUMO	0.24861
			HOMO to LUMO	-0.29781
3	614.4	0.0059	HOMO-6 to LUMO	0.11958
			HOMO-5 to LUMO	-0.27979
			HOMO-3 to LUMO	-0.17925
			HOMO-2 to LUMO	0.12584
			HOMO-1 to LUMO	0.59000
4	573.6	0.3194	HOMO-6 to LUMO	-0.12255
			HOMO-4 to LUMO	0.35380
			HOMO to LUMO	0.57535

Table S11. The 36 lowest energy singlet states for L^{H}CuOH structure computed at the TD-B98/6-311+G(d,p)/SDD level of theory.

Excited State	Excitation Energy (nm)	Oscillator Strength
1	599.2	0.0008
2	588.2	0.0020
3	564.4	0.0013
4	546.1	0.3194
5	508.3	0.0038
6	461.9	0.0001
7	441.6	0.0401
8	413.3	0.0000
9	395.8	0.0341
10	387.7	0.0002
11	362.2	0.0000
12	360.2	0.0007
13	355.4	0.0037
14	352.9	0.0154
15	343.7	0.0000
16	340.9	0.0001
17	334.5	0.0286
18	333.3	0.0000
19	325.2	0.0018
20	321.5	0.0026
21	317.6	0.0005
22	311.0	0.0000
23	308.5	0.0000
24	305.1	0.0000
25	300.2	0.0645
26	294.2	0.0000
27	291.4	0.0212
28	285.0	0.0187
29	284.8	0.0000
30	281.1	0.0093
31	279.3	0.0000
32	275.6	0.0001
33	273.9	0.0000
34	270.1	0.0071
35	267.1	0.0000
36	264.6	0.0006

Table S12. The 36 lowest energy singlet states for L^{OMe}CuOH structure computed at the TD-B98/6-311+G(d,p)/SDD level of theory.

Excited State	Excitation Energy (nm)	Oscillator Strength
1	587.8	0.0011
2	580.8	0.0012
3	554.8	0.0029
4	537.1	0.3197
5	499.7	0.0039
6	467.4	0.0006
7	436.9	0.0438
8	392.1	0.0382
9	372.9	0.0000
10	353.7	0.0001
11	352.6	0.0016
12	350.4	0.0140
13	332.3	0.0284
14	330.5	0.0001
15	325.0	0.0007
16	322.6	0.0075
17	320.3	0.0007
18	319.4	0.0000
19	316.5	0.0003
20	314.3	0.0005
21	309.9	0.0001
22	303.3	0.0002
23	302.7	0.0050
24	301.3	0.0004
25	299.2	0.0003
26	296.5	0.0545
27	289.8	0.0000
28	288.7	0.0371
29	277.9	0.0116
30	276.7	0.0000
31	273.5	0.0001
32	270.2	0.0150
33	268.2	0.0000
34	267.0	0.0172
35	263.2	0.0082
36	262.9	0.0000

Table S13. The 36 lowest energy singlet states for $L^{H}CuOCH_2CF_3$ structure computed at the TD-B98/6-311+G(d,p)/SDD level of theory.

Excited State	Excitation Energy (nm)	Oscillator Strength
1	679.3	0.0555
2	678.0	0.0012
3	627.0	0.0049
4	578.7	0.3222
5	559.7	0.0093
6	524.0	0.0241
7	454.1	0.0743
8	433.4	0.0242
9	414.7	0.0007
10	397.1	0.0136
11	373.1	0.0021
12	364.2	0.0157
13	359.5	0.0027
14	352.2	0.0017
15	349.1	0.0001
16	348.1	0.0008
17	343.5	0.0034
18	336.8	0.0001
19	330.0	0.0017
20	328.4	0.0005
21	323.9	0.0046
22	311.7	0.0043
23	311.2	0.0020
24	309.4	0.0001
25	307.0	0.0252
26	304.8	0.0025
27	303.2	0.0208
28	298.3	0.0023
29	297.2	0.0037
30	295.9	0.0029
31	293.3	0.0007
32	291.4	0.0840
33	289.1	0.0229
34	284.5	0.0026
35	280.0	0.0353
36	278.4	0.0103

Table S14. The 36 lowest energy singlet states for $L^{OMe}CuOCH_2CF_3$ structure computed at the TD-B98/6-311+G(d,p)/SDD level of theory.

Excited State	Excitation Energy (nm)	Oscillator Strength
1	674.9	0.0199
2	665.4	0.0299
3	614.4	0.0059
4	573.6	0.3194
5	552.0	0.0143
6	525.8	0.0269
7	451.8	0.0855
8	430.9	0.0255
9	394.3	0.0184
10	374.3	0.0029
11	359.3	0.0098
12	353.6	0.0043
13	352.2	0.0002
14	348.0	0.0003
15	342.1	0.0015
16	330.9	0.0003
17	323.3	0.0021
18	320.6	0.0002
19	317.9	0.0001
20	315.7	0.0041
21	309.5	0.0027
22	306.9	0.0006
23	306.6	0.0002
24	304.2	0.0283
25	301.3	0.0005
26	299.4	0.0474
27	296.2	0.0056
28	295.3	0.0028
29	292.3	0.0005
30	291.1	0.0006
31	289.5	0.0743
32	286.5	0.0059
33	280.0	0.0078
34	277.9	0.0838
35	275.5	0.0006
36	275.1	0.0158

DFT Frontier Molecular Orbitals

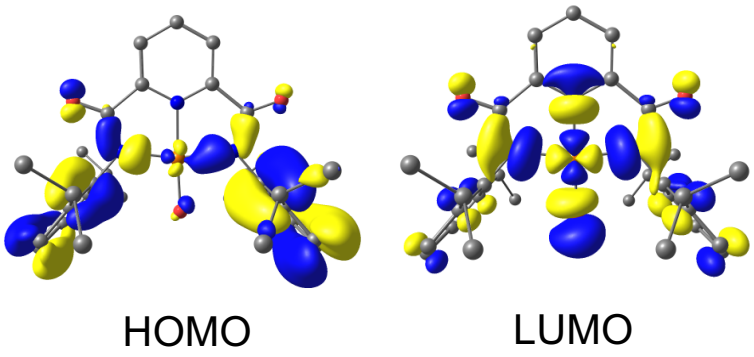

Figure S51. Selected molecule orbitals from the L^{H}CuOH structure computed at the B98/6-311+G(d,p)/SDD level of theory. Orbitals are plotted with an isovalue of 0.03 a.u. Hydrogen atoms, with the exception of the OH group, are excluded for clarity.

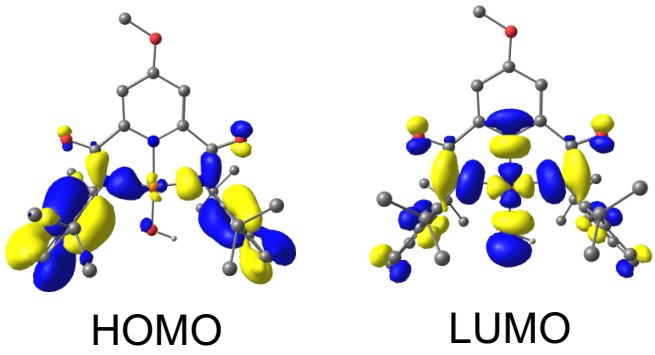

Figure S52. Selected molecule orbitals from the L^{OMe}CuOH structure computed at the B98/6-311+G(d,p)/SDD level of theory. Orbitals are plotted with an isovalue of 0.03 a.u. Hydrogen atoms, with the exception of the OH group, are excluded for clarity. C in grey, Cu in orange, O in red, N in blue, and H in white.

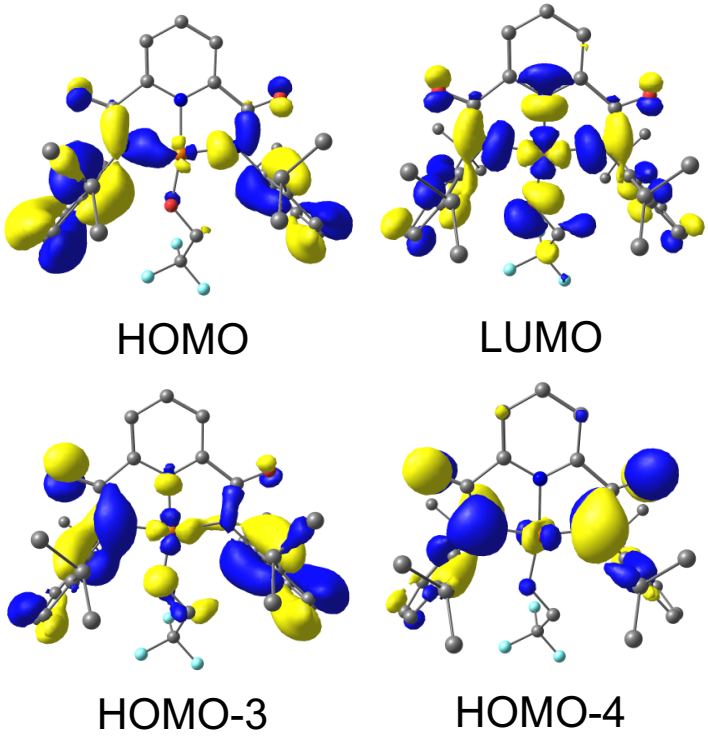

Figure S53. Selected molecule orbitals from the $L^{H}CuOCH_2CF_3$ structure computed at the B98/6-311+G(d,p)/SDD level of theory. Orbitals are plotted with an isovalue of 0.03 a.u. Hydrogen atoms are excluded for clarity. C in grey, Cu in orange, O in red, N in blue, and F in cyan.

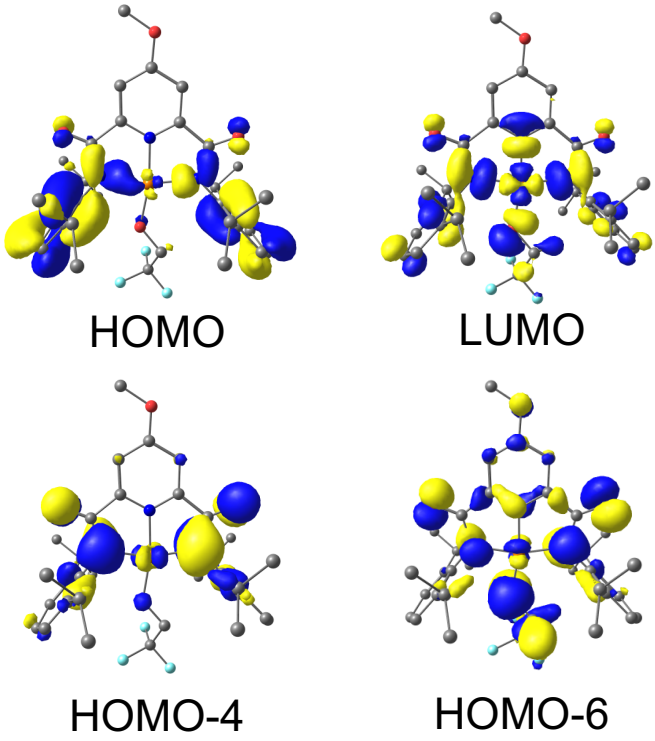

Figure S54. Selected molecule orbitals from the $L^{OMe}CuOCH_2CF_3$ structure computed at the B98/6-311+G(d,p)/SDD level of theory. Orbitals are plotted with an isovalue of 0.03 a.u. Hydrogen atoms are excluded for clarity. C in grey, Cu in orange, O in red, N in blue, and F in cyan.

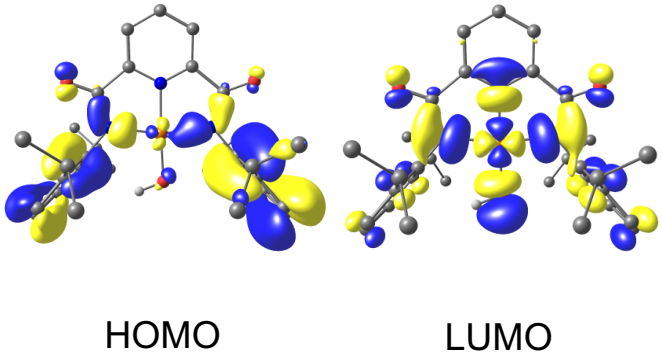

Figure S55. Selected molecule orbitals from the $L^{H}CuOH$ structure computed at the *m*PWPW91/6-311+G(d,p)/SDD level of theory. Orbitals are plotted with an isovalue of 0.03 a.u. Hydrogen atoms, with the exception of the OH group, are excluded for clarity.

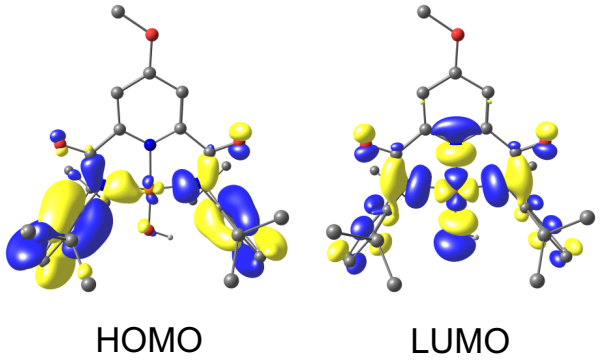

Figure S56. Selected molecule orbitals from the $L^{OMe}CuOH$ structure computed at the *m*PWPW91/6-311+G(d,p)/SDD level of theory. Orbitals are plotted with an isovalue of 0.03 a.u. Hydrogen atoms, with the exception of the OH group, are excluded for clarity. C in grey, Cu in orange, O in red, N in blue, and H in white.

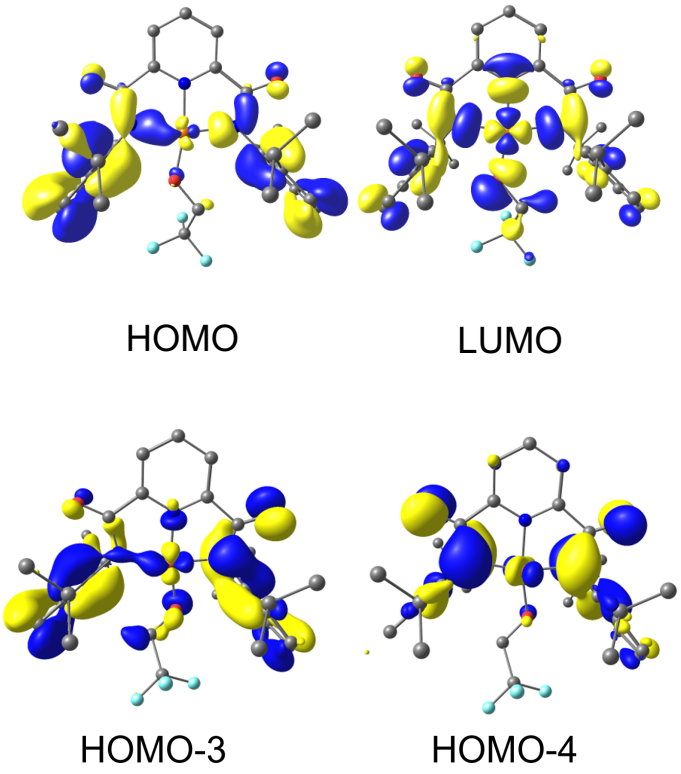

Figure S57. Selected molecule orbitals from the $L^{H}CuOCH_2CF_3$ structure computed at the *m*PWPW91/6-311+G(d,p)/SDD level of theory. Orbitals are plotted with an isovalue of 0.03 a.u. Hydrogen atoms are excluded for clarity. C in grey, Cu in orange, O in red, N in blue, and F in cyan.

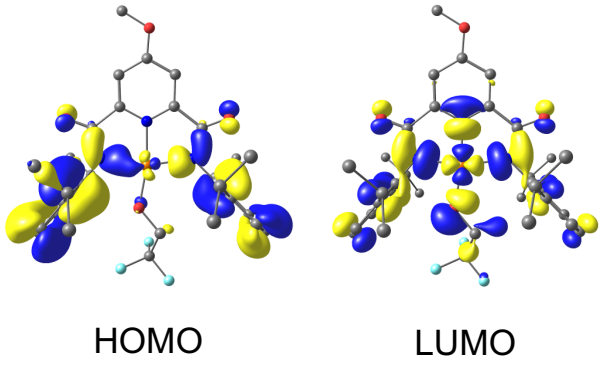

Figure S58. Selected molecule orbitals from the $L^{OMe}CuOCH_2CF_3$ structure computed at the *m*PWPW91/6-311+G(d,p)/SDD level of theory. Orbitals are plotted with an isovalue of 0.03 a.u. Hydrogen atoms are excluded for clarity. C in grey, Cu in orange, O in red, N in blue, and F in cyan.

DFT Raman Spectra

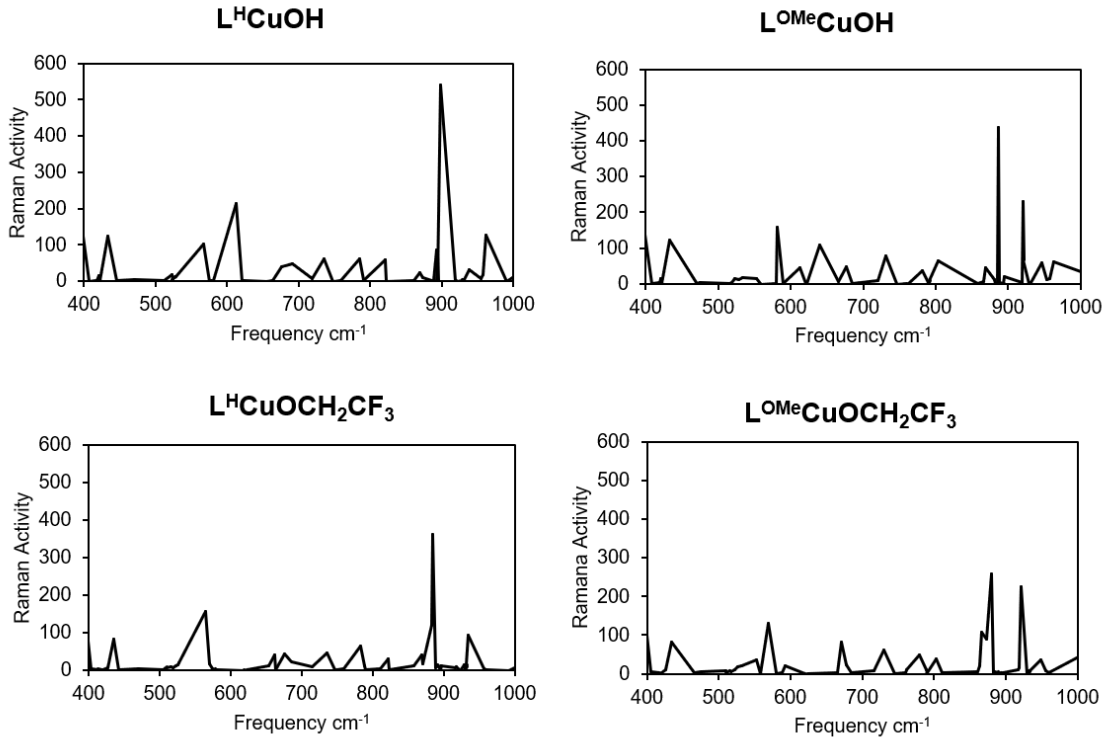

Figure S59. Raman Spectra obtained at MPWPW01/6-311+G(d,p)/SDD level of theory. Scaling factor for frequencies is set at 0.957.

Table S15. Vibrational frequencies (cm^{-1}) in the region of interest with non-zero Raman activities. Multiple modes contain contributions from Cu-OR stretches. Additionally modes with Cu-N motions are also observed. [a]Assigned as n_{Cu-OR}. [b]Assigned as n_{Cu-N}.

Complex	Frequency cm^{-1} (scaled)	Raman Activity(A^4/a.u)
$L^{H}CuOH$	613.3[a]	214.6
	676.5[b]	40.2
	691.1[b]	47.2
	898.5[b]	540.0
	259.2[b]	174.6
$L^{OMe}CuOH$	392.8[b]	217.1
	432.7[b]	122.7
	581.44[a]	159.4
	612.2[a]	44.1
	639.6[a]	109.3
	677.2[a]	47.0
	886.3[b]	438.7
$L^{H}CuOCH_2CF_3$	516.5[a]	10.7
	564.5[b]	155.4
	569.5[a]	18.6
	662.3[a]	41.9
	685.3[a]	23.7
	885.1[b]	360.9
	1060.2[b]	61.5
$L^{OMe}CuOCH_2CF_3$	393.9[a]	195
	509.5[a]	9.2
	510.6[a]	3.4
	515.9[a]	7.1
	568.6[a]	129.6
	670.9[b]	83.0
	880.1[b]	258.1
	873.2[b]	88.8

XIII. REFERENCES

[1] Maeder, M.; King, P. Reactlab, Jplus Consulting Pty Ltd: East Freemantle, WA. Australia, 2009.

[2] Connelly, N. G.; Geiger, W. E. "Chemical Redox Agents for Organometallic Chemistry." *Chem. Rev.* **1996**, *96 (2)*, 877-910.

[3] Spinney, H. A.; Clough, C. R.; Cummins, C. C., The titanium tris-anilide cation [Ti(N[(t)Bu]Ar)3](+) stabilized as its perfluoro-tetra-phenylborate salt: structural characterization and synthesis in connection with redox activity of 4,4'-bipyridine dititanium complexes. *Dalton Trans* **2015,** *44* (15), 6784-96.

[4] Thomson, R. K.; Scott, B. L.; Morris, D. E.; Kiplinger, J. L. "Synthesis, structure, spectroscopy and redox energetics of a series of uranium(IV) mixed-ligand metallocene complexes." *C. R. Chimie* **2010**, *13* (6), 790-802.

[5] Donoghue, P. J.; Tehranchi, J.; Cramer, C. J.; Sarangi, R.; Solomon, E. I.; Tolman, W. B., Rapid C–H Bond Activation by a Monocopper(III)–Hydroxide Complex. *Journal of the American Chemical Society* **2011,** *133* (44), 17602-17605.

[6] Sanning, J.; Ewen, P. R.; Stegemann, L.; Schmidt, J.; Daniliuc, C. G.; Koch, T.; Doltsinis, N. L.; Wegner, D.; Strassert, C. A., Scanning-Tunneling-Spectroscopy-Directed Design of Tailored Deep-Blue Emitters. *Angewandte Chemie International Edition* **2015,** *54* (3), 786-791.

[7] Stoll, S.; Schweiger, A. "EasySpin, a comprehensive software package for spectral simulation and analysis in EPR." *J. Magn. Reson.* **2006**, *178* (1), 42-55.

[8] A 60 mL syringe was equipped with a PTFE syringe filter and packed with basic alumina to the 15 mL mark; CH_2Cl_2 was passed through and immediately used.

[9] Dhar, D.; Yee, G. M.; Spaeth, A. D.; Boyce, D. W.; Zhang, H.; Dereli, B.; Cramer, C. J.; Tolman, W. B., Perturbing the Copper(III)-Hydroxide Unit through Ligand Structural Variation. *J. Am. Chem. Soc.* **2016,** *138* (1), 356-68.

[10] Zerk, T. J.; Saouma, C. T.; Mayer, J. M.; Tolman, W. B., Low Reorganization Energy for Electron Self-Exchange by a Formally Copper(III,II) Redox Couple. *Inorganic Chemistry* **2019,** *58* (20), 14151-14158.

[11] Bruker, 2012. Bruker AXS Inc., Madison, Wisconsin, USA.

[12] Bruker, 2001. Bruker AXS Inc., Madison, Wisconsin, USA.

[13] Sheldrick, G. M., "SHELXT – Integrated space-group and crystal structure determination," *Acta. Cryst.* **2015**, *A71*, 3–8.

[14] Sheldrick, G. M., "A short history of SHELX," Acta. Cryst. 2008, A64, 112–122.

[15] Dolomanov, O.V.; Bourhis, L.J.; Gildea, R.J.; Howard, J.A.K.; Puschmann, H., "OLEX2: A complete structure solution, refinement and analysis program," *J. Appl. Cryst*. **2009**, *42*, 339–341.

[16] Hubschle, C. B.; Sheldrick, G. M.; Dittrich, B., "ShelXle: a Qt graphical interface for SHELXL," *J. Appl. Cryst.* **2011**, *44*, 1281–1284.

[17] F. Menges "Spectragryph - optical spectroscopy software", Version 1.2.14, 2020, http://www.effemm2.de/spectragryph/

[18] Spaeth, A. D.; Gagnon, N. L.; Dhar, D.; Yee, G. M.; Tolman, W. B., Determination of the Cu(III)-OH Bond Distance by Resonance Raman Spectroscopy Using a Normalized Version of Badger's Rule. *J Am Chem Soc* **2017,** *139* (12), 4477-4485.

[19] Hayes, E. C.; Porter, T. R.; Barrows, C. J.; Kaminsky, W.; Mayer, J. M.; Stoll, S., Electronic Structure of a CuII–Alkoxide Complex Modeling Intermediates in Copper-Catalyzed Alcohol Oxidations. *Journal of the American Chemical Society* **2016,** *138* (12), 4132-4145.

[20] C. Adamo and V. Barone, "Exchange functionals with improved long-range behavior and adiabatic connection methods without adjustable parameters: The mPW and mPW1PW models," *J. Chem. Phys.*, **1998**, *108*, 664-675. DOI: 10.1063/1.475428

[21] Gaussian 16, Revision A.03, M. J. Frisch, G. W. Trucks, H. B. Schlegel, G. E. Scuseria, M. A. Robb, J. R. Cheeseman, G. Scalmani, V. Barone, G. A. Petersson, H. Nakatsuji, X. Li, M. Caricato, A. V. Marenich, J. Bloino, B. G. Janesko, R. Gomperts, B. Mennucci, H. P. Hratchian, J. V. Ortiz, A. F. Izmaylov, J. L. Sonnenberg, D. Williams-Young, F. Ding, F. Lipparini, F. Egidi, J. Goings, B. Peng, A. Petrone, T. Henderson, D. Ranasinghe, V. G. Zakrzewski, J. Gao, N. Rega, G. Zheng, W. Liang, M. Hada, M. Ehara, K. Toyota, R. Fukuda, J. Hasegawa, M. Ishida, T. Nakajima, Y. Honda, O. Kitao, H. Nakai, T. Vreven, K. Throssell, J. A. Montgomery, Jr., J. E. Peralta, F. Ogliaro, M. J. Bearpark, J. J. Heyd, E. N. Brothers, K. N. Kudin, V. N. Staroverov, T. A. Keith, R. Kobayashi, J. Normand, K. Raghavachari, A. P. Rendell, J. C. Burant, S. S. Iyengar, J. Tomasi, M. Cossi, J. M. Millam, M. Klene, C. Adamo, R. Cammi, J. W. Ochterski, R. L. Martin, K. Morokuma, O. Farkas, J. B. Foresman, and D. J. Fox, Gaussian, Inc., Wallingford CT, 2016.

[22] Dolg, M.; Wedig, U.; Stoll, H.; Preuss, H. Energy-Adjusted Abinitio Pseudopotentials for the First Row Transition Elements. *J. Chem. Phys*. **1987**, *86*, 866-872.

[23] Clark, T.; Chandrasekhar, J.; Spitznagel, G. W.; Schleyer, P. V. R. Efficient Diffuse Function-Augmented Basis Sets for Anion Calculations. III. The 3-21+G Basis Set for First-Row Elements, Li-F. **1983**, *4*, 294-301.

[24] Krishnan, R.; Binkley, J. S.; Seeger, R.; Pople, J. A. Self-consistent molecular orbital methods. XX. A basis set for correlated wave functions. *J. Chem. Phys*. **1980**, *72*, 650-654.

[25] Precomputed vibrational scaling factors. https://cccbdb.nist.gov/vibscalejust.asp (accessed Dec 26, 2020).

[26] Becke, A. D. "Density-functional thermochemistry. V. Systematic optimization of exchange-correlation functionals," *J. Chem. Phys.*, **1997**, *107*, 8554-8560.

[27] Schmider, H. L.; Becke, A. D. "Optimized density functionals from the extended G2 test set," *J. Chem. Phys.*, **1998**, *108*, 9624-9231.